Chemical Physics 472 (2016) 142–155

Contents lists available at ScienceDirect

Chemical Physics

journal homepage: www.elsevier.com/locate/chemphys

The role of halogen C–$X_1\cdots X_2$–C contact on the preferred conformation of 2-perhalomethylchromones in solid state

C.D. Alcívar León [a,1], G.A. Echeverría [b], O.E. Piro [b], S.E. Ulic [a,c,*], J.L. Jios [d,*], M. Burgos Paci [e], G.A Argüello [e]

[a] CEQUINOR (CONICET-UNLP), Facultad de Ciencias Exactas, Universidad Nacional de La Plata, 47 esq. 115, 1900 La Plata, Argentina
[b] Departamento de Física, Facultad de Ciencias Exactas, Universidad Nacional de La Plata e IFLP (CONICET, CCT-La Plata), C. C. 67, 1900 La Plata, Argentina
[c] Departamento de Ciencias Básicas, Universidad Nacional de Luján, Rutas 5 y 7, 6700 Luján, Buenos Aires, Argentina
[d] UNIDAD PLAPIMU-LASEISIC (UNLP-CIC), Departamento de Química, Facultad de Ciencias Exactas, Universidad Nacional de La Plata, 47 esq. 115, 1900 La Plata, Argentina
[e] INFIQC, Departamento de Físico Química, Facultad de Ciencias Químicas, Universidad Nacional de Córdoba, Córdoba, Argentina

ARTICLE INFO

Article history:
Received 6 January 2016
In final form 23 March 2016
Available online 7 April 2016

Keywords:
2-Chlorodifluoromethylchromones
Halogen–halogen contacts
Single crystal X-ray diffraction
Spectroscopic properties
Quantum chemical calculations

ABSTRACT

The solid state of 2-chlorodifluoromethyl-3-methylchromone (**1**) and 3-bromomethyl-2-chlorodifluoromethylchromone (**2**) was studied by vibrational spectroscopy (IR, Raman) and X-ray diffraction methods. The analysis was extended to solution phase using UV–Vis, NMR (^{1}H, ^{13}C and ^{19}F) and fluorescence spectroscopy with the assistance of theoretical calculations. The crystal structure of **2** shows chlorine and bromine atoms of the $-CF_2Cl$ and $-CH_2Br$ groups on the same side of the molecular plane, while in the most stable conformer predicted by theoretical calculations, these halogen atoms are opposite. These differences were interpreted in terms of intra- and intermolecular interactions in the crystal packing. Particularly, the weak non covalent halogen–halogen contact plays a decisive role in the preferred conformation adopted in solid phase. In addition, results of fluorescence spectroscopy are in accordance with the X-ray spectroscopy, since the proposed association due to intermolecular interactions was also found in solution when the concentration of **2** was increased.

1. Introduction

The structural ring of chromone is prevailing in nature [1]. Chromones were greatly studied by the diversity of its applications in industries, such as pharmaceuticals and agrochemicals [2,3]. They show to be nutraceutical [4] and exhibit diverse biological properties [5–9]. In fact there are several studies on the potential pharmaceutical activity of structural analogs of chromone [6,10,11]. They are the structural unit of the title compounds (**1**) and (**2**) synthesized and characterized in this work. As is well known, the introduction of electronegative substituents such as trihalomethyl groups (CX_3; X = F, Cl) involves the rearrangement of the electron density in the molecule and therefore changes in the reactivity towards nucleophilic reagents [12]. Moreover, the substitution of hydrogen by fluorine is one of the most commonly employed monovalent isosteric replacements [13]. The introduction of heavy halogen atoms (Cl, Br), generates steric changes in the molecule which may influence the structural properties. The bulky bromine atom showed a strong effect on the crystal packing in related haloalkylated chromones [14].

On the other hand, halogen···halogen interactions have been object of substantial discussion over recent years. Research derived from the Cambridge Structural Database [15–17] suggested the appearance of two kinds of interactions taking into account the C—X···X′ and C—X′···X angles, θ_1 and θ_2. The interaction is termed as type I when $\theta_1 \approx \theta_2$, and type II when $\theta_1 = 180°$ and $\theta_2 = 90°$. Most examples of type I come from interactions through a crystallographic symmetry center, and those with a linear system C–X···X–C are limited. Type II interactions are originated by the polarizability of the halogen, increasing from chlorine to iodine.

This "halogen bonding" is relevant in the field of supramolecular chemistry [18,19]. Due to its high directionality [20], they are of wide applicability [21–25] and in addition to its role in structural chemistry, they also influence the physical properties of crystalline materials [26–30].

The main difference in the pharmacological properties of molecules, where hydrogen has been substituted for fluorine, is probably linked to the difference in electronegativity between both

* Corresponding authors at: CEQUINOR (CONICET-UNLP), Facultad de Ciencias Exactas, Universidad Nacional de La Plata, 47 esq. 115, 1900 La Plata, Argentina (S.E. Ulic). UNIDAD PLAPIMU-LASEISIC (UNLP-CIC), Departamento de Química, Facultad de Ciencias Exactas, Universidad Nacional de La Plata, 47 esq. 115, 1900 La Plata, Argentina (J.L. Jios).

E-mail addresses: sonia@quimica.unlp.edu.ar (S.E. Ulic), jljios@quimica.unlp.edu.ar (J.L. Jios).

[1] SENESCYT-Ecuador.

http://dx.doi.org/10.1016/j.chemphys.2016.03.017
0301-0104/

elements. According to LaVoie, the differences in pharmacological activities can be attributed to the influence of the electron-withdrawing ($-I$) effect that the fluorine substitution causes on interaction with either a biological receptor or enzyme, as well as its effect on the metabolic fate of the drug [13]. The improvement in physicochemical properties such as lipophilicity leads to an enhanced lipid solubility (bioavailability), and increases the attractiveness of fluorine-containing molecules as potential drugs [31,32]. The fluorescence properties of chromones were widely studied and depend on the different groups attached to the chromone skeleton [33–38]. The reactivity and luminescence properties of a group of brominated chromones were also investigated [39]. Recently 3-alkyl-6-methoxy-7-hydroxychromones have been proposed for biological imaging [40].

Some 2-perfluoroalkylcromones closely related to the title compounds were synthesized by intramolecular cyclization of β-phenoxypropenoic acids, using an excess of 85% PPA, as dehydrating agent, at high temperatures [41]. Other 2-polyfluoroalkylated chromones were obtained by intramolecular Friedel–Crafts acylation of the Z isomers of 3-(aryloxy)polyfluoro-2-alkenoic acids [42]. However, the aforementioned methods lack stereo-specificity and produce mixtures of isomers or destruction of intermediates. More recently, 2-trifluoromethylchromones were obtained and studied using spectroscopic methods and theoretical calculations [43]. Moreover, none of them allows to access to 3-substituted chromones. In this work, the title molecule 2-chlorodifluoromethyl-3-methylchromone (**1**) was obtained in moderate yield with a one-pot synthetic method [44]. 3-Bromomethyl-2-chlorodifluoromethylchromone (**2**) was synthesized by mono-bromination of the methyl group [14]. To the best of our knowledge, these are the first study of 3-substituted 2-chlorodifluoromethylchromones. The structures of the title compounds are shown in Scheme 1.

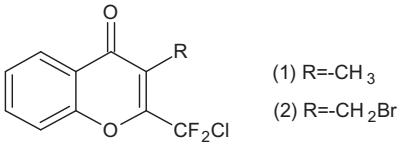

Scheme 1. Structures of the title compounds.

2. Experimental

2-Chlorodifluoromethylchromones **1** and **2** were synthesized according to previous reported methods.[14,44] NMR, CG-MS, IR and Raman, UV–Vis, and fluorescence spectra were measure to characterize both compounds. Besides, the crystal structures of **1** and **2** were determined by X-ray diffraction methods. The gas phase geometry optimization of both molecules was performed by quantum chemical calculations. Additional theoretical studies were selected for calculating vibrational frequencies (IR, Raman), UV–Vis transitions and NMR chemical shifts (^{1}H, ^{13}C).

2.1. Instrumentation

2.1.1. Infrared and Raman spectroscopy

Infrared absorption spectra (KBr pellets) were recorded on a LUMEX InfraLUM FT-02 spectrometer with a resolution of 2 cm^{-1} in the range from 4000 to 400 cm^{-1}. Raman dispersion spectra of the solid were measured from powdered samples in Pyrex standard capillaries (2.5 mm i.d.) with a Perkin-Elmer FT-Raman RFs 100/s spectrometer using, as exciting light source, the 1064 nm line from a Nd/YAG laser (spectral resolution of 4 cm^{-1}) in the 3500–100 cm^{-1} spectral range.

2.1.2. NMR spectra

The ^{1}H, ^{19}F and ^{13}CNMR spectra of (**1**) were recorded at 25 °C with a Bruker Avance II 500 spectrometer. The samples were dissolved in $CDCl_3$ and the solution introduced within a 5 mm NMR tube. Chemical shifts (δ) are given in parts per million (ppm) relative to tetramethylsilane (TMS, $\delta = 0$ ppm). For the ^{19}F NMR spectrum a 0.05% TFA in $CDCl_3$ solution was used as external reference ($\delta = -71.0$ ppm). Coupling constants (J) are reported in Hz, and the multiplicity was signalized as: *s* (singlet), *d* (doublet), *dd* (double doublet), *ddd* (double double doublet), *t* (triplet), *q* (quartet) and *br.d* (broad doublet) (see Section 2.2). For NMR data, the standard numbering scheme of the benzopyran skeleton (with the bridged oxygen atom carrying the number 1) was adopted to facilitate the comparison with data reported in the literature. The ^{1}H and ^{13}C NMR spectra of **1** and **2** are shown in Figs. S1 and S2 (Supporting Information).

2.1.3. UV–visible spectroscopy

The spectra of **1** and **2** in methanol were recorded using a quartz cell (10 mm optical path length) on a ChromTech CT-5700 UV/Vis spectrophotometer at 2.0 nm spectral bandwidth. Measurements were carried out in the spectral region from 190 to 1100 nm.

2.1.4. Mass spectrometry

The MS determinations were performed by injection of methanol solutions (~1 μl) in a HP 5890 Chromatograph coupled to a HP 5972A mass selective detector. An HP5-MS capillary column (30 m × 0.25 mm × 5 μm) has been used with H_2 as the carrier gas (0.6 ml/min). The temperature set points were: 200 °C in the split injector, 300 °C in the interface, 185 °C in the ion source, the oven ramp started at 80 °C and ended at 200 °C with a heating rate of 10 °C/min. The electron energy was 70 eV with a mass range of 50–350 amu and a pressure in the mass spectrometer lower than 10^{-5} Torr. The mass spectra of **1** and **2** are shown in Figs. S3 and S4 (Supporting Information).

2.1.5. X-ray diffraction data

The measurements were performed on an Oxford Xcalibur Gemini, Eos CCD diffractometer with graphite-monochromated CuKα ($\lambda = 1.54178$ Å) radiation. X-ray diffraction intensities were collected (ω scans with ϑ and κ-offsets), integrated and scaled with CrysAlisPro [45] suite of programs. The unit cell parameters were obtained by least-squares refinement (based on the angular setting for all collected reflections with intensities larger than seven times the standard deviation of measurement errors) using CrysAlisPro. Data were corrected empirically for absorption employing the multi-scan method implemented in CrysAlisPro and in the case of **1** also for extinction. The structures were solved by direct methods with SHELXS-97 of the SHELX suite of programs [46] and the molecular model refined by full-matrix least-squares procedure with SHELXL-97 of the same package. Hydrogen atoms were positioned on stereo-chemical basis and refined with the riding model. The methyl H-atoms of **1** were positioned by treating the —CH_3 moiety as a rigid group allowed to rotate around the corresponding C—CH_3 bond such as to maximize the residual electron density at the calculated H-positions. At this stage, the determination of the absolute structure of **1** by the Flack's procedure [47] implemented in SHELXL-97 showed that the crystal was in fact an almost perfect racemic twin.

Crystal data and structure refinement results are summarized in Table 1. Crystallographic structural data have been deposited at the Cambridge Crystallographic Data Centre (CCDC). Any request to the Cambridge Crystallographic Data Centre for this material should quote the full literature citation and the reference number CCDC 1409239 (**1**) and CCDC 1409240 (**2**).

Table 1
Crystal data and structure refinement results for **1** and **2**.

	1	**2**
Empirical formula	C_{11} H_7 Cl F_2 O_2	C_{11} H_6 Br Cl F_2 O_2
Formula weight	244.62	323.52
Temperature (K)	297(2)	297(2)
Wavelength (Å)	1.54184	1.54184
Crystal system	Orthorhombic	Triclinic
Space group	$P2_12_12_1$	$P-1$
Unit cell dimensions		
a (Å)	5.1483(4)	7.5457(9)
b (Å)	7.3422(7)	12.4441(12)
c (Å)	27.394(2)	14.0915(13)
α (°)	90.0	111.301(9)
β (°)	90.0	104.074(9)
γ (°)	90.0	99.741(9)
Volume (Å^3)	1035.5(2)	1146.2(2)
Z, density (calculated, Mg/m^3)	4, 1.569	4, 1.875
Absorption coefficient (mm^{-1})	3.414	7.202
F(000)	496	632
Crystal shape/color	Plate/colorless	Plate/colorless
Crystal size (mm^3)	0.409 × 0.197 × 0.085	0.563 × 0.218 × 0.046
ϑ-Range (°) for data collection	6.24–68.98	3.57–71.99
Index ranges	$-6 \leqslant h \leqslant 3$, $-7 \leqslant k \leqslant 8$, $-25 \leqslant l \leqslant 33$	$-5 \leqslant h \leqslant 9$, $-15 \leqslant k \leqslant 13$, $-17 \leqslant l \leqslant 17$
Reflections collected	2453	8368
Independent reflections	1690 [R(int) = 0.0191]	4470 [R(int) = 0.0313]
Observed reflections [$I > 2\sigma(I)$]	1253	2741
Completeness (%) to ϑ = 71.98°	99.9	98.8
Refinement method	Full-matrix least-squares on F^2	Full-matrix least-squares on F^2
Data/restraints/parameters	1690/0/148	4470/0/307
Goodness-of-fit on F^2	1.050	1.174
Final R indices[a] [$I > 2\sigma(I)$]	R_1 = 0.0450, wR_2 = 0.0999	R_1 = 0.0954, wR_2 = 0.2887
R indices (all data)	R_1 = 0.0684, wR_2 = 0.1204	R_1 = 0.1300, wR_2 = 0.3444
Largest diff. peak and hole (e Å^{-3})	0.173 and −0.202	2.227 and −1.253

[a] $R_1 = \Sigma||F_o| - |F_c||/\Sigma|F_o|$, $wR_2 = [\Sigma w(|F_o|^2 - |F_c|^2)^2/\Sigma w(|F_o|^2)^2]^{1/2}$.

2.1.6. Fluorescence spectroscopy

Steady-state fluorescence measurements were carried out using a PTI-QM2 spectrometer from Photon Technology International. The excitations as well as the emission slits of both monochromators were set to obtain a spectral resolution of 0.5 nm. The excitation source was a 75 Watt Xe lamp, and the luminescence intensity was recorded with a photon counter detector. An initial scan was carried out to locate the emission range and immediately after, the exit monochromator was set to a fixed wavelength and the excitation spectrum was recorded. Once the maximum of excitation was found, the fluorescence emission spectra were recorded always at the maximum wavelength.

2.2. Synthesis

*2.2.1. 2-Chlorodifluoromethyl-3-methylchromone (**1**) [44]*

In a round-bottom flask with ground glass joint, 2′-hydroxypropiophenone (8.9 g; 57.9 mmol) and pyridine (4.8 ml) were added with stirring until complete dissolution. Then, chlorodifluoroacetic anhydride (5.6 g; 22.96 mmol) was incorporated and the solution was refluxed (bath temperature 130 °C) with constant stirring for 10 h. After cooling, a dark red viscous reaction mixture was obtained. It was partitioned in 60 ml of dichloromethane and 10 ml of 0.3 M hydrochloric acid. The phases were only partially separated after leaving to stand overnight and subsequent centrifugation. The remaining aqueous phase containing undissolved solids and residual organic phase was extracted with hexane (4 × 20 ml). The organic portions were combined, dried with Na_2SO_4 and the solvents were removed with a rotary evaporator to give a waxy violet colored solid. The product was purified by flash chromatography (hexane/ethyl acetate, 19:1) yielding a white solid. Recrystallization from hot hexane gives a crystalline solid.

^{1}H NMR (500 MHz, $CDCl_3$) δ = 8.18 (*dd*, 1H, H-5, J = 8 and 1.5 Hz), 7.71 (*ddd*, 1H, H-7, J = 8.5, 7 and 1.5 Hz), 7.49 (*dd*, 1H, H-8, J = 8.5 and 0.5 Hz), 7.42 (*ddd*, 1H, H-6, J = 8, 7 and 1 Hz), 2.24 ppm (*t*, 3H, CH_3, $^5J_{H,F}$ = 3 Hz). ^{13}C RMN (126 MHz, $CDCl_3$) δ = 178.1 (C-4), 154.9 (C-8a), 151.8 (t, C-2, $^2J_{C,F}$ = 30 Hz), 134.6 (C-7), 126.2 (C-6), 125.9 (C-5), 122.2 (C-4a), 121.8 (*t*, CF_2Cl, $^1J_{C,F}$ = 293.5 Hz), 118.9 (C-3), 118.2 (C-8), 9.0 (*t*, CH_3, $^4J_{C,F}$ = 4 Hz). ^{19}F RMN (471 MHz, $CDCl_3$) δ = −54.1 ppm. MS: m/z (%) = 244 ([M]$^+$, 74), 209 ([M−Cl]$^+$, 91), 208 ([M−HCl]$^+$, 64), 181 ([$C_{10}H_7O_2F_2$]$^+$, 100), 159 ([$C_{10}H_7O_2$]$^+$, 7), 131 ([$C_9H_7O_2$]$^+$, 21), 120 ([$C_7H_4O_2$]$^+$, 10), 92 ([C_6H_4O]$^+$, 40), 76 ([C_6H_4]$^+$, 9), 63 ([C_5H_3]$^+$, 40), 50 ([CF_2]$^+$, 17). UV–Vis (methanol), λ: 205, 228, 250 and 309 nm.

*2.2.2. 3-Bromomethyl-2-chlorodifluoromethylchromone (**2**)*

In a bottom flask with ground glass joint, 0.96 g (2.96 mmol) of (**1**) was dissolved in 30 ml of carbon tetrachloride. Then, 100 ml of saturated aqueous solution of bromine was added, and the mixture was sealed with a rubber stopper and kept with stirring at room temperature under visible light irradiation for 24 h (monitored by TLC). The organic phase was separated, dried (with Na_2SO_4) and the solvent removed with a rotary evaporator yielding **2** as a white solid in quantitative yield. Recrystallization from methanol resulted in a white crystalline solid.

^{1}H NMR (500 MHz, $CDCl_3$) δ = 8.24 (*dd*, 1H, H-5, ^3J = 8 and 1.5 Hz), 7.79 (*ddd*, 1H, H-7, ^3J = 8.5, 7 and 1.5 Hz), 7.55 (*d*, 1H, H-8, ^3J = 8.5 Hz), 7.50 (*t*, 1H, H-6, J = 7.5 Hz), 4.61 ppm (*s*, 2H, CH_2Br). ^{13}C RMN (126 MHz, $CDCl_3$) δ = 175.7 (C-4), 154.8 (C-8a), 153.5 (*t*, C-2, $^2J_{C,F}$ = 31 Hz), 135.3 (C-7), 126.7 (C-5), 126.5 (C-6), 122.5 (C-4a), 121.2 (*t*, CF_2Cl, $^1J_{C,F}$ = 294 Hz), 119.3 (C-3), 118.4 (C-8), 19.3 ppm (*t*, CH_2Br, $^4J_{C,F}$ = 5 Hz). ^{19}F RMN (471 MHz, $CDCl_3$) δ = −55.3 ppm. MS: m/z (%) = 323 ([M]$^+$, 0.5), 288 ([M−Cl]$^+$, 0.5), 287 ([M−HCl]$^+$, 12), 244 ([M−Br]$^+$, 15), 243 ([M−HBr]$^+$, 77), 208 ([$C_{11}H_6F_2O_2$]$^+$,

100), 120 ($[C_7H_4O_2]^+$, 64), 92 ($[C_6H_4O]^+$, 65), 50 ($[CF_2]^+$, 14). UV–Vis (methanol), λ: 205, 232, 259 and 305 nm.

2.3. Computational methods

Quantum chemical calculations were performed for the ground state (gas phase) of both molecules with the program package Gaussian 09 [48]. Scans of the potential energy surface, geometry optimizations, electrostatic potential surfaces and vibrational frequency calculations were carried out with the Density Functional Theory (B3LYP) method employing the 6-311++G(d,p) basis set. In all cases, the calculated vibrational properties correspond to potential energy minima with no imaginary values for the frequencies. The ^{1}H and ^{13}C chemical shifts were calculated with B3LYP/6-311+g(2d,p) optimized geometries by the GIAO method (Gauge Including Atomic Orbital), using the corresponding TMS shielding calculated at the same level of theory. Moreover, scans, geometry optimizations and calculation of electronic transitions were calculated within the framework of the Time-Dependent DFT [49,50] using the B3LYP functional and the 6-311++G(d,p) basis set and the conductor-like polarisable continuum model (CPCM) of methanol [51,52]. Furthermore, for **2** the potential energy surface was calculated with B3LYP/6-311++g(d,p) level of theory for the ground state, where scans were performed around the dihedral angles involving the heavy bromine and chlorine atoms (OC–CCl and CC–CBr).

3. Results and discussion

3.1. Crystallographic structural results

Figs. 1 and 2 are ORTEP [53] drawings of **1** and **2** molecules and their bond distances and angles are in Table 2. Due to extended π-bonding the chromone molecular skeleton in both moieties are planar (*rms* deviation of non-H atoms from the corresponding best least-squares planes equal to 0.045 Å for **1** and less than 0.032 Å for **2**).

3.1.1. Compound *1*

The fluorine and chlorine atoms are at opposite sides of the molecular plane [the fluorine atoms at 0.528(5) and 0.620(4) Å and the chlorine at 1.691(3) Å measured perpendicularly from the best least-squares molecular plane]. Observed bond distances and angles agree with Organic Chemistry rules. In fact, within the phenyl ring C—C distances [from 1.361(7) to 1.381(5) Å] are as expected for a resonant-bond structure. The fused heterocycle shows a C8—C9 bond length of 1.343(5) Å, shorter than the other heterocycle C—C distances [1.453(5) and 1.467(6) Å], which corresponds to a formally double bond character for that link (see Fig. 1). C—O single bond distances are 1.352(4) and 1.384(4) Å, and carbonyl C=O double bond length is equal to 1.231(4) Å. The —C(sp^3)F_2Cl group exhibits the expected tetrahedral bonding structure with C—C—X angles from 110.3(4)° to 112.0(3)° and X—C—X angles in the 106.2(4)–108.4(3)° range. Observed C—F bond distances are 1.339(5) and 1.331(5) Å, and d(C—Cl) = 1.745 (4) Å.

3.1.2. Compound *2*

There are two independent but structurally closely related molecules in the crystal asymmetric unit (moieties #1 and #2). In fact, the *rms* separation between homologous non-H atoms in the best least-square fitting, calculated by the Kabsh procedure [54] is 0.079 Å. Chlorine and bromine atoms on the —CF_2Cl and —CH_2Br groups are at the same side of the molecular planes.

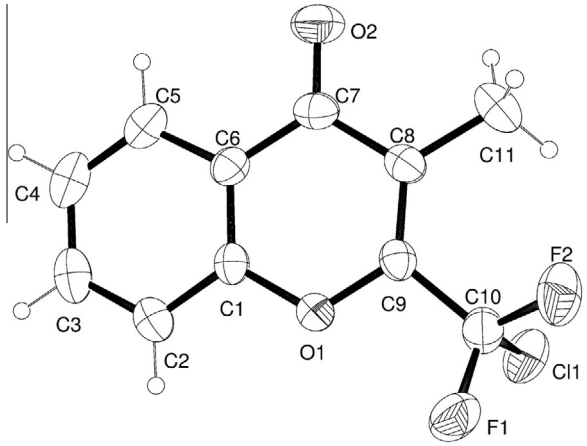

Fig. 1. View of 2-clorodifluoromethyl-3-methylchromone (1) molecule showing the labeling of the non-H atoms and their displacement ellipsoids at the 30% probability level.

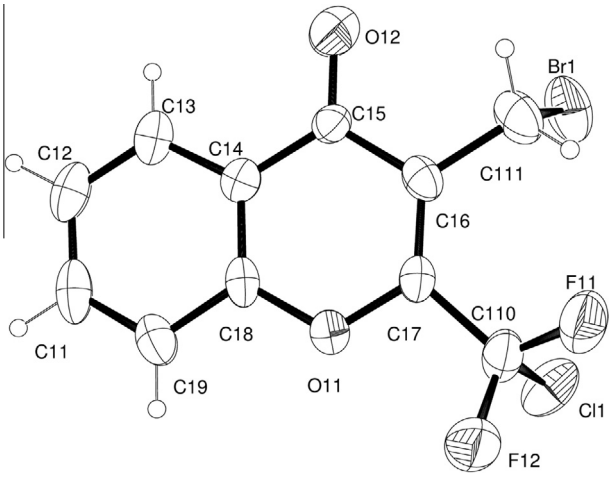

Fig. 2. View of 3-bromomethyl-2-chlorodifluoromethylchromone (2) molecule showing the labeling of the non-H atoms and their displacement ellipsoids at the 30% probability level.

As expected, observed bond distances and angles within the chromone fragments and the —C(sp^3)F_2Cl group agree with each other and with the corresponding ones of the related and better refined **1** compound, and therefore they would not be discussed here any further. The —C(sp^3)H_2Br groups exhibit a tetrahedral bonding structure with C—C—Br bond angles of 110.0(7)° (#1) and 111.6(6)° (#2) and C—Br bond lengths of 1.950(9) Å (#1) and 1.962(9) Å (#2).

3.2. Structural properties

Potential energy curves (B3LYP/6-311++g(d,p)) for internal rotation around the —CF_2Cl, —CH_3 and —CH_2Br groups for **1** and **2**, respectively, were carried out to assess the minimum energy molecular geometry adopted by both compounds in the gas phase (see Fig. 3). The molecules are characterized by a planar conformation. Potential energy curves for the OC–CCl dihedral angle of **1** and **2** are compared in Fig. 4a. The scan around the —CF_2Cl group shows two equivalent energy minima at 90.0° and 270.0° for **1**, and two minima at 80.0° and 290.0° for **2** (being the last minimum 0.19 kcal/mol higher in energy). The scan around the —CH_2Br

Table 2
Experimental and calculated bond lengths [Å], bond angles [°], and selected torsion angles [°][a,b] of **1** and **2**.

Param.	**1**		Param.	**1**		Param.	**2**		Param.	**2**	
	Exp.	Calc.		Exp.	Calc.		Exp.	Calc.		Exp.	Calc.
r(C1–C6)	1.381(5)	1.396	∠(C4–C5–C6)	120.3(4)	120.4	*r*(C11–C19)	1.350(1)	1.385	∠(C13–C14–C15)	122.8(7)	121.7
r (C1–O1)	1.384(4)	1.367	∠(C1–C6–C5)	117.8(4)	118.4	*r*(C11–C12)	1.377(2)	1.404	∠(O12–C15–C16)	119.8(7)	121.6
r(C1–C2)	1.377(5)	1.397	∠(C1–C6–C7)	119.8(4)	119.9	*r*(C12–C13)	1.369(1)	1.383	∠(O12–C15–C14)	122.8(7)	122.8
r(C2–C3)	1.379(6)	1.385	∠(C5–C6–C7)	122.4(4)	121.7	*r*(C13–C14)	1.388(1)	1.405	∠(C16–C15–C14)	117.4(6)	115.6
r(C3–C4)	1.380(6)	1.405	∠(O2–C7–C8)	121.0(4)	121.8	*r*(C14–C18)	1.379(1)	1.395	∠(C17–C16–C15)	119.0(7)	118.4
r(C4)–C5)	1.361(7)	1.383	∠(O2–C7–C6)	122.2(4)	122.6	*r*(C14–C15)	1.447(1)	1.472	∠(C17–C16–C111)	124.4(8)	126.4
r(C5–C6)	1.391(6)	1.405	∠(C8–C7–C6)	116.8(4)	115.6	*r*(C15–O12)	1.246(1)	1.222	∠(C15–C16–C111)	124.4(8)	115.2
r(C6–C7)	1.453(5)	1.474	∠(C9–C8–C7)	117.6(4)	118.1	*r*(C15–C16)	1.444(1)	1.490	∠(C16–C17–O11)	123.7(7)	124.5
r(C7–O2)	1.231(4)	1.224	∠(C9–C8–C11)	125.0(4)	125.3	*r*(C16–C17)	1.342(1)	1.356	∠(C16–C17–C110)	129.2(7)	128.2
r(C7–C8)	1.467(6)	1.483	∠(C7–C8–C11)	117.4(4)	116.6	*r*(C16–C111)	1.499(1)	1.492	∠(O11–C17–C110)	107.0(7)	107.3
r(C8–C9)	1.343(5)	1.353	∠(C8–C9–O1)	126.0(4)	125.3	*r*(C17–O11)	1.358(9)	1.349	∠(O11–C18–C14)	121.3(6)	121.1
r(C8–C11)	1.496(5)	1.505	∠(C8–C9–C10)	125.6(4)	125.8	*r*(C17–C110)	1.506(1)	1.522	∠(O11–C18–C19)	117.0(8)	116.8
r(C9–O1)	1.352(4)	1.354	∠(O1–C9–C10)	108.2(3)	108.8	*r*(C18–O11)	1.376(9)	1.369	∠(C14–C18–C19)	121.7(8)	122.1
r(C9–C10)	1.512(5)	1.519	∠(F2–C10–F1)	106.2(4)	107.1	*r*(C18–C19)	1.409(1)	1.395	∠(C11–C19–C18)	117.1(9)	118.4
r(C10–F2)	1.331(5)	1.348	∠(F2–C10–C9)	111.7(4)	111.5	*r*(C110–F11)	1.322(1)	1.346	∠(F11–C110–F12)	103.9(8)	106.9
r(C10–F1)	1.339(5)	1.346	∠(F1–C10–C9)	110.3(4)	110.9	*r*(C110–F12)	1.340(1)	1.350	∠(F11–C110–C17)	112.3(8)	112.4
r(C10–Cl1)	1.745(4)	1.806	∠(F2–C10–Cl1)	108.4(3)	108.1	*r*(C110–Cl1)	1.755(9)	1.795	∠(F12–C110–C17)	111.8(7)	109.8
∠(C6–C1–O1)	121.4(4)	121.2	∠(F1–C10–Cl1)	108.0(3)	107.9	*r*(C111–Br1)	1.950(9)	1.999	∠(F11–C110–Cl1)	106.7(6)	108.4
∠(C6–C1–C2)	122.6(4)	121.9	∠(C9–C10–Cl1)	112.0(3)	111.2	∠(C19–C11–C12)	123.1(9)	120.8	∠(F12–C110–Cl1)	107.9(7)	108.3
∠(O1–C1–C2)	116.0(4)	116.8	∠(C9–O1–C1)	118.4(3)	119.7	∠(C13–C12–C11)	118.8(8)	120.1	∠(C17–C110–Cl1)	113.6(7)	110.9
∠(C1–C2–C3)	118.1(4)	118.5	Φ(O1–C9–C10–Cl1)	91.95	90.0	∠(C12–C13–C14)	121.0(9)	120.3	∠(C16–C111–Br1)	110.0(7)	111.3
∠(C4–C3–C2)	120.2(5)	120.7	Φ(C7–C8–C11–H11a)	86.76	90.6	∠(C18–C14–C13)	118.1(7)	118.5	∠(C17–O11–C18)	119.6(6)	120.5
∠(C5–C4–C3)	120.9(5)	120.0	Φ(C8–C9–C10–F1)	156.68	151.6	∠(C18–C14–C15)	119.1(7)	119.8	Φ(C(17–C16–C111–Br1)	92.96	86.7

[a] Atom numbering scheme taken from Figs. 1 and 2.
[b] Experimental data from X-ray diffraction and computed parameters at the B3LYP/6-311++g(d,p) level of theory.

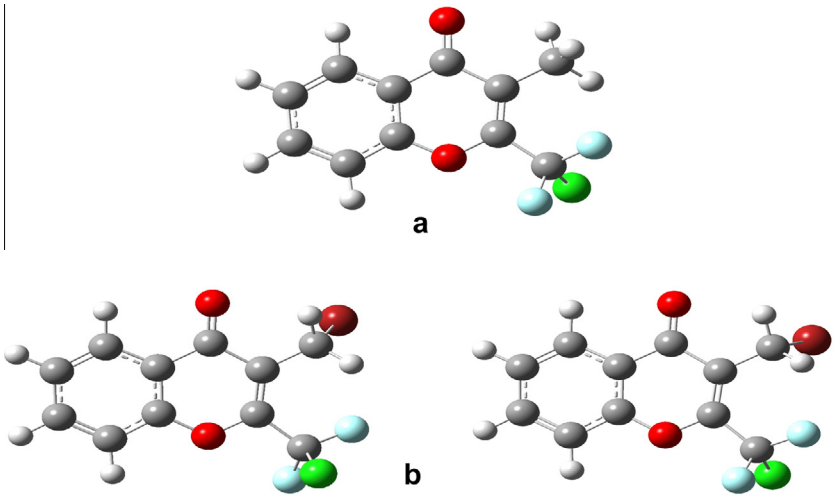

Fig. 3. Optimized structures (B3LYP/6-311++g(d,p)) of (a) **1** and (b) **2**.

group (Fig. 4b) for **2** has two equivalent energy minima around 88° and 267°.

Fig. 3 shows the most stable conformers of **1** and **2** after geometry optimization, based on the potential energy curves. The chlorine atom arranges perpendicular (OC–CCl = 90.0°) in **1** and almost perpendicular and on the opposite side in **2** (OC–CCl = 278°), both relative to the C=C bond. For **2**, the bromine atom is perpendicular to the molecular plane (CC–CBr = 272°).

Comparing the conformational preferences of both compounds in the gas phase (calculated) and solid phase (experimental), a great difference was found between them. In Fig. 5 the molecular packing of **1** is displayed. Along the two fold screw axis, CF_2Cl groups pack with the Cl1 and F1 atoms at a distance of 3.356 (4) Å; the C10–Cl1···F1^{i} and C10–F1···Cl1^{ii} angles are 141.3(2) and 117.3(3)°, respectively. The Cl1···F1^{i} distance is slightly longer than the Van der Waals radii sum of Cl and F atoms. Although some influence on molecular packing could be expected, they will not be enough to overcome intramolecular interactions, resulting in a molecular conformation close to that of the gas phase.

The packing of **2** is presented in Fig. 6, where dashed lines are used to show some relevant intermolecular contacts. Their geometries, listed in Table 3, are near to the expected values for halogen···halogen contact [18,19] and hydrogen bonds [55], and therefore could be considered as attractive. Furthermore, along the *a* axis, molecules are arranged in a face to face offset stacking at a ring distances of 3.530 Å and some π stacking interaction might be also expected. As is discussed below (see Potential Energy Surface section), the most stable conformation in the gas phase has the chlorine and bromine atoms directed towards the opposite side of the molecular plane. Although the configuration with both halogen atoms oriented to the same side is higher in energy, this difference is exceeded by the multiple interactions found in the crystal

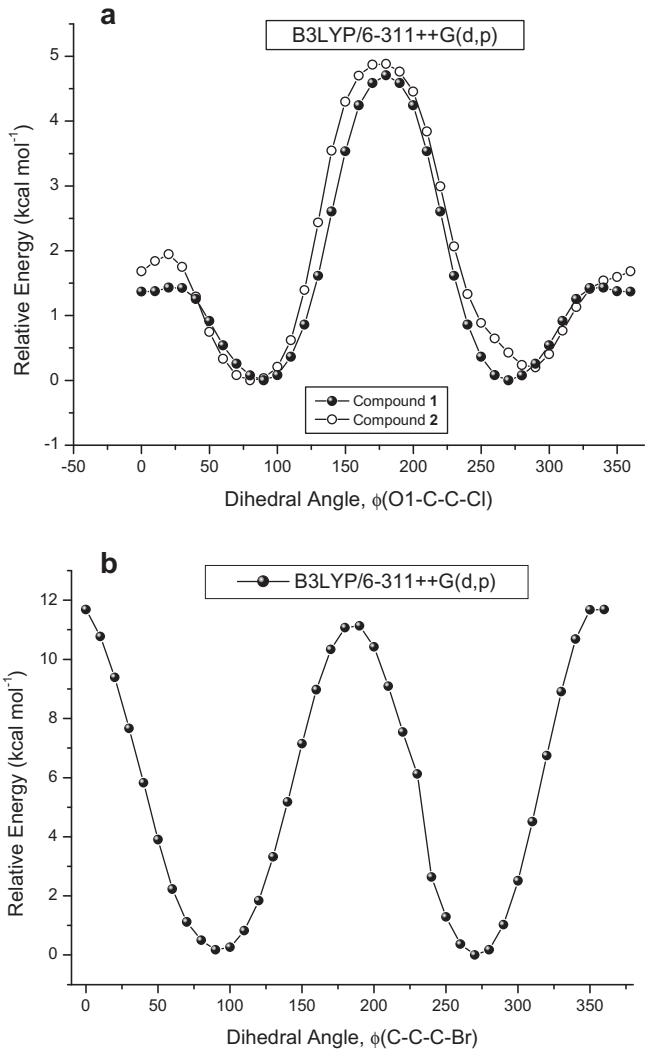

Fig. 4. (a) Potential energy curve for the internal rotation around the dihedral angle ϕ(O1—C—C—Cl) bond in **1** and **2**, calculated at the B3LYP/6-311++G(d,p) level of theory. (b) Potential energy curve for the internal rotation around the C—C16—C111—Br bond in **2**, calculated at the B3LYP/6-311++G(d,p) level of theory.

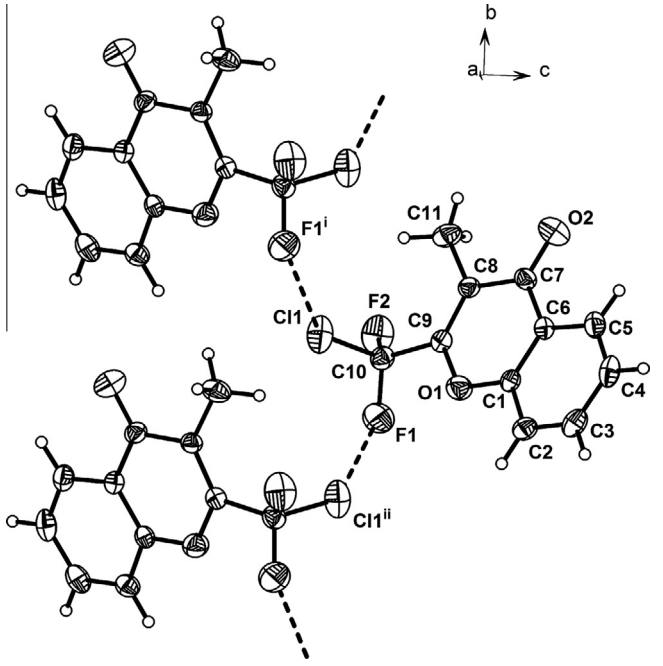

Fig. 5. View of the molecular packing of 2-clorodifluoromethyl-3-methylchromone showing the labeling of the non-H atoms and their displacement ellipsoids at the 30% probability level. In dashed line is depicted the Cl···F contact. Symmetry operations: (i) $1-x, 0.5+y, 0.5-z$; (ii) $1-x, -0.5+y, 0.5-z$.

packing. Particularly for **2**, the weak halogen–halogen contacts seem to be the most relevant interactions, since they act cooperatively in the stacking of the molecules (C–Cl···Cl–C, and C–Br···Br–C). These contacts can be described as type I, since the experimental angles (θ_1 and θ_2) are approximately equal (see Table 3).

3.3. Potential energy surface

The potential energy surface scan [B3LYP/6-311++g(d,p)] for compound **2** was performed over the OC–CCl and CC–CBr torsion angles, (see Fig. S10 of S. I.). The surface shows clearly two minima. The global minimum, corresponding to the conformation having the bromine and chlorine atoms perpendicular to the fused rings plane but on opposite sides (OC–CCl = −81.8°; CC–CBr = −87.8°), while the second conformation is 0.176 kcal/mol higher in energy and is distinguishable only for the arrangement of the both halogen atoms on the same side of the plane (OC–CCl = 73.8°; CC–CBr = −92.7°). In spite of its higher energy, the last conformation matches very well with the molecular geometry found in X-ray diffraction (OC–CCl = 91.45°; CC–CBr = −88.92°). Moreover, the percent population based on Gibbs free energies and Maxwell–Boltzmann statistics shows that the both conformers are almost equally populated in gas phase 57% and 43%. Probably, additional stabilization due to intermolecular interaction in the crystal packing leads to the configuration of higher energy as the preferred conformation in the crystal. Additional evidences found in solution support this positive intermolecular associative effect (see Fluorescence Spectra section).

3.4. Vibrational spectroscopy

The experimental IR and Raman spectra of **1** and **2** (solid state) are presented in Figs. 7 and 8, respectively. Tables 4 and 5 show the observed fundamental vibrational modes of **1** and **2**, together with a tentative assignment. They were performed by inspection of the corresponding calculated spectra and reported values of related compounds. Only the most relevant functional groups of the molecules will be discussed.

3.4.1. 2-Chlorodifluoromethyl-3-methylchromone (*1*)

The bands corresponding to the —CH_3 group were observed in the IR spectrum at 3049, 2970 and 2935 cm^{-1} (Raman, 3020, 2975 and 2938 cm^{-1}) and assigned to the asymmetric and symmetric stretching modes. Moreover, the CH_3 angular deformations modes were attributed to the IR bands at 1469, 1436 and 1395 cm^{-1} (Raman, 1472, 1441 and 1397 cm^{-1}), assigned to both asymmetric and symmetric deformations, respectively. Also, the vibrational rocking mode appeared at 1058 cm^{-1} in the Raman spectrum (Calc.: 1059 cm^{-1}) but it was not observed in the IR spectrum.

The 4-pyran moiety showed the corresponding band of the carbonyl group at 1649 cm^{-1} and at 1648 cm^{-1} (Calc: 1705 cm^{-1}) in the IR and Raman spectra, respectively. The C=C stretching bond was attributed to the band at 1611 cm^{-1} in IR (Raman, 1612 cm^{-1}).

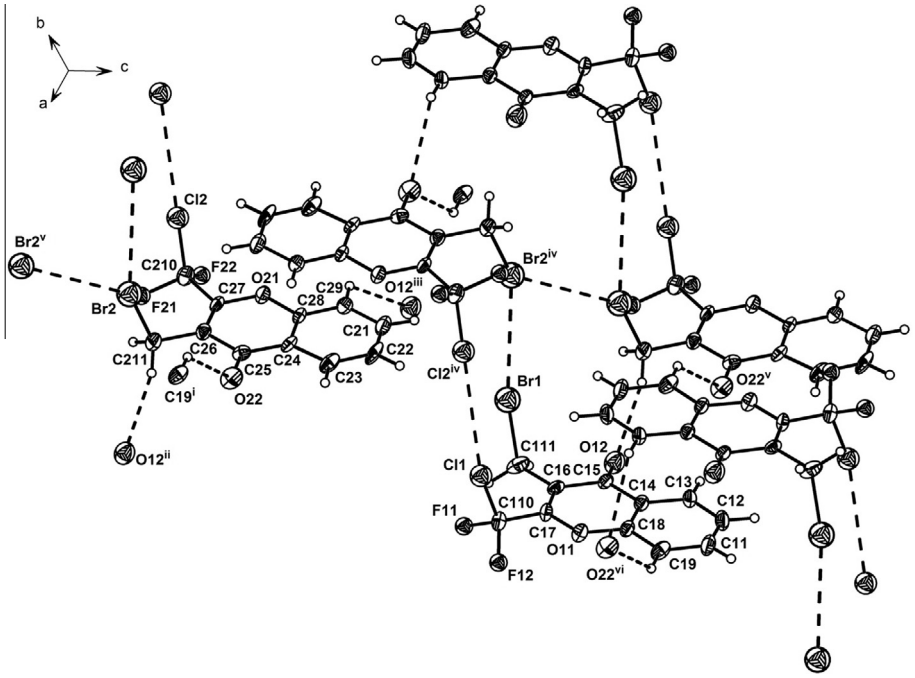

Fig. 6. Molecular packing for 3-bromomethyl-2-chlorodifluoromethylchromone. In dashed lines are shown intermolecular halogen···halogen contacts and hydrogen bonds. Symmetry operations are listed in Table 3.

Table 3
Selected intra-e intermolecular contacts for **2** [Å and °].

D–X···A–Y contacts	D–X/A–Y[a]	X···A	D···A	D–X···A	X···A–Y
C111–H11A···F11–C110	0.97/1.31(1)	2.26	2.93(1)	125.5	103.4
C211–H21B···F21–C210	0.97/1.36(2)	2.17	2.84(2)	125.1	107.0
C19–H19···O22^{i}–C25^{i}	0.93/1.23(1)	2.62	3.33(1)	133.5	130.7
C211–H21A···O12^{ii}–C15^{ii}	0.97/1.224(9)	2.48	3.41(1)	162.7	134.4
C29–H29···O12^{iii}–C15^{iii}	0.93/1.224(9)	2.62	3.21(1)	122.0	131.8
C111–Br1···Br2^{iv}–C211^{iv}	1.95(1)/1.96(1)	3.621(2)	–	169.2(4)	144.9(4)
C211–Br2···Br2^{v}–C211^{v}	1.96(1)/1.96(1)	3.664(2)	–	139.7(4)	139.7(4)
C110–Cl1···Cl2^{iv}–C210^{iv}	1.76(1)/1.73(1)	3.619(6)	–	151.7(4)	174.6(4)

Symmetry transformations used to generate equivalent atoms: (i) $-x, -y, -z+1$; (ii) $x, y, z-1$ (iii) $-x+1, -y+1, -z+2$; (iv) $-x, 1-y, 1-z$; (v) $-x, 1-y, -z$.
[a] X = H, Br or Cl and A = O, Br or Cl.

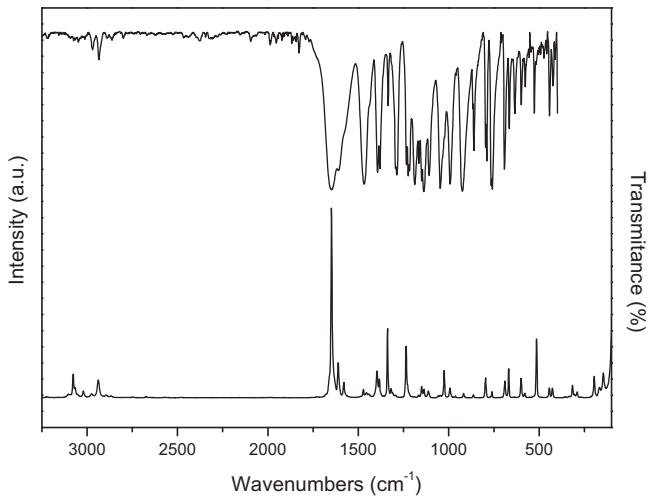

Fig. 7. Infrared spectrum of the solid (upper trace, KBr pellets) and Raman spectrum (lower trace) of 2-chlorodifluoromethyl-3-methylchromone (**1**) at room temperature.

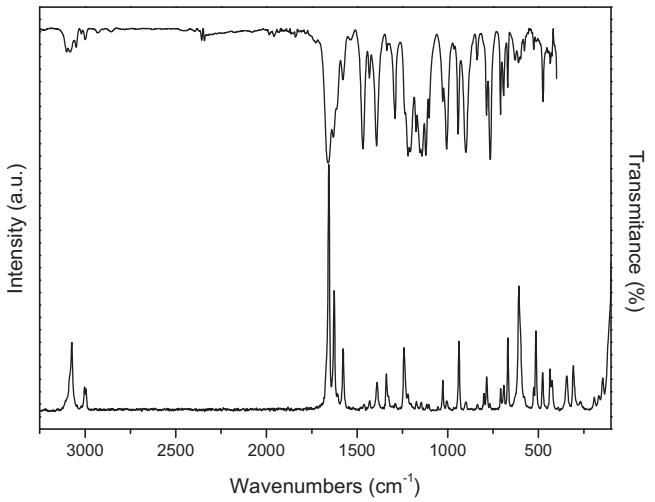

Fig. 8. Infrared spectrum of the solid (upper trace, KBr pellets) and Raman spectrum (lower trace) of 3-bromomethyl-2-chlorodifluoromethylchromone (**2**) at room temperature.

Table 4
Experimental and calculated frequencies (cm^{-1}) and tentative assignment of fundamental vibration modes in 2-chlorodifluoromethyl-3-methylchromone (**1**).

Mode	Experimental		Calculated[b]		Assignment[c]
	IR[a]	Raman	Frequency	Intensity	
ν_1	3274(vw)	3077(13)	3205	6	ν(C5–H)$_{iph}$; ν(C4–H)$_{iph}$; ν(C3–H)$_{iph}$; ν(C2–H)$_{iph}$
ν_2	–	–	3202	2	ν(C5–H)$_{iph}$; ν(C4–H)$_{iph}$; ν(C3–H)$_{oph}$; ν(C2–H)$_{oph}$
ν_3	3222(vw)	3066(6)	3189	6	ν(C5–H)$_{iph}$; ν(C4–H)$_{oph}$; ν(C3–H)$_{oph}$; ν(C2–H)$_{iph}$
ν_4	3074(vw)	3053(2)	3176	3	ν(C5–H)$_{iph}$; ν(C4–H)$_{oph}$; ν(C3–H)$_{iph}$; ν(C2–H)$_{oph}$
ν_5	3049(vw)	3020(4)	3145	3	ν_{as}(CH$_3$)
ν_6	2970(vw)	2975(2)	3109	7	ν_{as}(CH$_3$)
ν_7	2935(vw)	2938(9)	3045	11	ν_s(CH$_3$)
ν_8	1649(vs)	1648(100)	1705	315	ν(C7–O2)
ν_9	1611(m)	1612(19)	1664	60	ν(C9–C8)
ν_{10}	1574^{sh}(m)	1604^{sh}(7)	1648	56	ν(C7–C6)$_{oph}$; ν(C5–C4)$_{iph}$; ν(C2–C1)$_{iph}$
ν_{11}	–	1483(1)	1613	11	ν(C4–C3)$_{oph}$; ν(C3–C2)$_{iph}$; δ(C5–C7–H)$_{ip}$; δ(C5–C7–H)$_{ip}$
ν_{12}	–	–	1503	2	δ(C4–C5–H)$_{ip}$; δ(C3–C2–H)$_{ip}$; δ(C6–C5–H)$_{ip}$; ν(C7–C6)
ν_{13}	1469(vs)	1472(4)	1495	119	δ_{as}(CH$_3$); δ(C5–C7–H)$_{ip}$; δ(C5–C4–H)$_{ip}$
ν_{14}	–	1455(3)	1493	14	δ(C5–C4–H)$_{ip}$; δ_{as}(CH$_3$)
ν_{15}	1436^{sh}(vw)	1441(2)	1480	13	δ_{as}(CH$_3$)
ν_{16}	1395(s)	1397(14)	1421	7	δ_s(CH$_3$)
ν_{17}	1382(s)	1383(10)	1400	93	δ(C8–C9–O1)$_{ip}$; ν(C8–C7); ν(C9–C10); δ_{as}(CH$_3$)
ν_{18}	1336(w)	1319(5)	1362	8	ν(C6–C1)$_{iph}$; ν(C7–C5)$_{iph}$; ν(C4–C3)$_{oph}$; ν(C2–C1)$_{oph}$
ν_{19}	1288(s)	–	1310	69	δ(C3–C2–H)$_{ip}$; δ(C4–C5–H)$_{ip}$
ν_{20}	1225(s)	1236(27)	1247	81	ν(C1–O1); δ(C3–C2–C1)$_{ip}$
ν_{21}	1218(s)	1228(7)	1235	35	ν(C7–C6); δ(C7–C6–C5)$_{ip}$; δ(C3–C4–H)$_{ip}$; δ(C3–C8–H)$_{ip}$
ν_{22}	1189(s)	1167(2)	1193	168	δ(C8–C11–H)$_{ip}$; ν(C9–C10)
ν_{23}	–	–	1179	30	δ(C3–C4–H)$_{ip}$; δ(C2–C3–H)$_{ip}$; ν(C9–O1)$_{iph}$; ν(C8–C11)$_{oph}$
ν_{24}	1166(m)	1150(6)	1166	32	δ(C4–C3–H)$_{ip}$; δ(C1–C2–H)$_{ip}$; ν(C9–O1)$_{iph}$; ν(C8–C11)$_{oph}$
ν_{25}	1139(vs)	1137(5)	1143	161	ν_{as}(CF$_2$); δ(C6–C5–H)$_{ip}$; δ(C3–C4–H)$_{ip}$; δ(C3–C4–H)$_{ip}$
ν_{26}	1109(m)	1113(4)	1125	55	δ(C4–C5–H)$_{ip}$; δ(C4–C3–H)$_{ip}$; δ(C1–C2–H)$_{ip}$
ν_{27}	–	1058(1)	1059	42	ρ_{rock}(CH$_3$)
ν_{28}	1148(vs)	1048(1)	1051	57	δ(C4–C3–H)$_{ip}$; δ(O1–C9–C8)$_{ip}$
ν_{29}	1134^{sh}(m)	1025(15)	1047	12	ν(C4–C3); δ(C4–C3–H)$_{ip}$; δ(C3–C2–H)$_{ip}$
ν_{30}	–	–	1006	<1	γ(C4–C5–H)$_{iph}$; γ(C3–C4–H)$_{oph}$; γ(C2–C3–H)$_{iph}$
ν_{31}	994(s)	993(5)	996	74	δ(C6–C7–O2)$_{ip}$; ρ_r(CH$_3$); γ(C9–C10–Cl)
ν_{32}	963(vw)	963(1)	983	2	γ(C4–C5–H)$_{iph}$; γ(C4–C3–H)$_{oph}$; γ(C3–C2–H)$_{iph}$
ν_{33}	926(vs)	918(2)	911	220	ν(C10–Cl); ρ_r(CH$_3$); δ(C6–C7–O2)
ν_{34}	868(w)	–	881	<1	γ(C6–C5–H)$_{iph}$; γ(C5–C4–H)$_{iph}$; γ(C3–C2–H)$_{oph}$
ν_{35}	862(w)	864(2)	875	6	δ(C5–C4–C3)$_{ip}$; δ(C1–O1–C9)$_{ip}$; ρ_{rock}(CH$_3$)
ν_{36}	798(m)	–	800	4	γ(C8–C7–C6)$_{oph}$; γ(C5–C4–H)$_{iph}$; γ(C4–C3–H)$_{iph}$
ν_{37}	791(m)	797(11)	799	53	δ(C8–C9–O1); ν(C10–Cl)
ν_{38}	760(s)	761(3)	772	68	γ(C7–C6–C1)$_{iph}$; γ(C4–C5–H)$_{iph}$; γ(C3–C4–H)$_{iph}$
ν_{39}	693(m)	–	707	17	γ(C5–C4–C3)$_{iph}$; γ(C7–C6–C1)$_{oph}$; γ(C8–C7–C6)$_{oph}$
ν_{40}	688^{sh}(w)	690(9)	696	8	δ(C4–C3–C2)$_{ip}$; ν(C8–C11); δ(C4–C3–C2)$_{ip}$; δ(O1–C9–C3)$_{ip}$
ν_{41}	667(vw)	669(15)	673	10	δ(CF$_2$); γ(O1–C9–C8); δ(C3–C2–C1)
ν_{42}	636(vw)	637(<1)	646	8	δ(C8–C7–O2)$_{ip}$; δ(O1–C1–C2)$_{ip}$; δ(C9–C8–C11)$_{ip}$
ν_{43}	600(vw)	600(10)	598	12	γ(O1–C9–C8); δ(C3–C2–C1)$_{ip}$
ν_{44}	578(vw)	580(2)	585	3	δ(C3–C2–C1)$_{ip}$; δ(C6–C5–C4)$_{ip}$; δ(CF$_2$)
ν_{45}	528(vw)	–	534	6	γ(C5–C4–C3); γ(C6–C1–C2)
ν_{46}	518(vw)	515(31)	519	2	δ(C7–C6–C1)$_{ip}$; δ(O1–C9–C8)$_{ip}$
ν_{47}	459(vw)	–	450	4	γ(C6–C5–C4); γ(C3–C2–C1)
ν_{48}	444(vw)	444(5)	442	5	δ(C7–C8–C9)$_{ip}$; δ(C1–O1–C9)$_{ip}$
ν_{49}	425(vw)	427(5)	423	3	δ(C8–C7–O2)$_{ip}$; δ(C2–C1–O1)$_{ip}$
ν_{50}	414 (vw)		415	2	γ(F–C–Cl); γ(C3–C2–C1)
ν_{51}	–	356(1)	358	5	δ(C11–C8–C7)$_{ip}$; δ(O2–C7–C6)$_{ip}$; γ(O1–C9–C10)
ν_{52}	–	336(1)	336	1	γ(C11–C8–C7); γ(C9–C10–Cl)
ν_{53}	–	316(7)	309	1	τ(O1–C9–C10–Cl); δ(C7–C6–C5)$_{ip}$; γ(C7–C8–C11)
ν_{54}	–	305(7)	301	<1	ρ_{tw}(CF$_2$); δ(C11–C8–C9)$_{ip}$
ν_{55}	–	290(3)	289	3	δ(C7–C6–C5)$_{ip}$; δ(C11–C8–C7)$_{ip}$
ν_{56}	–	–	264	2	ρ_{wag}(CF$_2$); τ(C9–C8–C11–H); τ(O1–C1–C6–C5)
ν_{57}	–	195(11)	186	1	γ(C9–C10–Cl); τ(C6–C1–C2–C3); τ(C8–C9–O1–C8a)
ν_{58}	–	167(6)	166	2	τ(CH$_3$); δ(O1–C9–C10)$_{ip}$
ν_{59}	–	145(13)	131	<1	τ(C7–C6–C1–C2); τ(O2–C7–C8–C11)
ν_{60}	–	–	98	1	τ(CH$_3$)
ν_{61}	–	–	75	5	τ(CH$_3$); τ(C8–C9–O1–C1)
ν_{62}	–	–	64	<1	τ(C8–C9–O1–C1); τ(C6–C1–C2–C3)
ν_{63}	–	–	20	<1	τ(C9–CF$_2$Cl); τ(CH$_3$)

[a] vs very strong; s, strong; m, medium; w, weak; vw, very weak; sh, shoulder.
[b] 6-311++g(d,p) calculated IR frequencies (cm^{-1}) and intensities (km mol^{-1}) in parentheses.
[c] ν, δ, γ, τ, ρ_{rock}, ρ_{wag} and ρ_{tw} represent stretching, in-plane deformation, out-of-plane deformation, torsion, rocking, wagging and twisting modes. In phase, in plane and out of phase modes are represented by iph, ip and oph, respectively.

The asymmetric stretching of the —CF_2 group was observed as an intense band at 1139 cm^{-1} (Calc.: 1143 cm^{-1}), while the Raman counterpart was located at 1137 cm^{-1}. The CF_2 bending appeared as a weak IR band at 667 cm^{-1} (Raman, 669 cm^{-1}), while the out of plane deformation showed up at 414 cm^{-1} (Calc.:415 cm^{-1}). Moreover, the twisting and wagging modes were predicted by the quantum chemical calculations at 301 and 264 cm^{-1}, respectively but only the twisting mode was observed in Raman at 305 cm^{-1}.

Table 5
Experimental and calculated frequencies (cm^{-1}) and tentative assignment of fundamental vibration modes in 3-bromomethyl-2-chlorodifluoromethylchromone (**2**).

Mode	Experimental		Calculated[b]		Assignment[c]
	IR[a]	Raman	Frequency	Intensity	
ν_1	–	–	3230	3	$\nu_{as}(CH_2)$
ν_2	3102(vw)	3073(28)	3207	5	ν(C13–H)$_{iph}$; ν(C12–H)$_{iph}$; ν(C11–H)$_{iph}$; ν(C19–H)$_{iph}$
ν_3	3081(vw)	3087^{sh}(14)|	3204	2	ν(C13–H)$_{iph}$; ν(C12–H)$_{oph}$; ν(C11–H)$_{oph}$; ν(C19–H)$_{iph}$
ν_4	3049(vw)	–	3191	6	ν(C13–H)$_{oph}$; ν(C12–H)$_{iph}$; ν(C11–H)$_{iph}$; ν(C19–H)$_{oph}$
ν_5	3020(vw)	3002(10)	3178	3	ν(C13–H)$_{iph}$; ν(C12–H)$_{oph}$; ν(C11–H)$_{iph}$; ν(C19–H)$_{oph}$
ν_6	2999(vw)	2994(10)	3145	3	$\nu_s(CH_2)$
ν_7	1660(vs)	1672(18)	1713	287	ν(C15–O12)
ν_8	1631(m)	1656(100)	1656	125	ν(C17–C16)
ν_9	1613^{sh}(m)	1626(49)	1645	8	ν(C17–C16)$_{iph}$; ν(C13–C12)$_{iph}$; ν(C11–C19)$_{iph}$
ν_{10}	1578(w)	–	1612	26	ν(C15–C18)$_{iph}$; ν(C12–C11)$_{iph}$; ν(C17–C16)$_{iph}$
ν_{11}	1536(vw)	1577(26)	1504	5	δ(C12–C13–H)$_{ip}$; δ(C11–C12–H)$_{ip}$; δ(C11–C19–H)$_{ip}$
ν_{12}	1468(m)	1462(3)	1494	123	δ(C13–C12–H)$_{ip}$; δ(C12–C11–H)$_{ip}$; δ(C11–C19–H)$_{ip}$
ν_{13}	1432(w)	1430(5)	1475	21	$\delta_s(CH_2)$
ν_{14}	1392(m)	1390(12)	1396	140	δ(C16–C111–H)$_{ip}$; δ(O1–C17–C16)$_{ip}$; δ(C11–C12–H)$_{ip}$; ν(C17–C110)
ν_{15}	1337(vw)	1339(15)	1361	21	δ(C14–C13–H)$_{ip}$; δ(C12–C11–H)$_{ip}$; δ(C18–C19–H)$_{ip}$; $\delta_{as}(CH_2)$
ν_{16}	1290(m)	1288(4)	1309	52	δ(C12–C13–H)$_{ip}$; δ(C11–C12–H)$_{ip}$; δ(C18–C19–H)$_{ip}$; δ(C18–C8–H)$_{ip}$
ν_{17}	1236(m)	1242(26)	1263	14	$\rho_w(CH_2)$
ν_{18}	1219(vs)	1219(7)	1247	106	δ(C14–C13–H)$_{ip}$; δ(C13–C12–H)$_{ip}$; δ(C19–C11–H)$_{ip}$; ν(O1–C18)
ν_{19}	1207(vs)	1202(3)	1238	31	δ(C13–C14–C18)$_{ip}$; δ(C12–C11–C19)$_{ip}$; $\rho_{tw}(CH_2)$
ν_{20}	1175(m)	1173(4)	1214	83	$\rho_{tw}(CH_2)$; ν(C17–C110)
ν_{21}	1154(vs)	1145(4)	1188	50	δ(C13–C12–H)$_{ip}$; δ(C19–C11–H)$_{ip}$; ν(C16–C111); ν(O1–C17)
ν_{22}	1143(vs)	1116(3)	1170	15	δ(C14–C13–H)$_{ip}$; δ(C13–C12–H)$_{ip}$; δ(C19–C11–H)$_{ip}$; δ(C18–C8–H)$_{ip}$
ν_{23}	1121(vs)	1104(3)	1149	162	$\nu_{as}(CF_2)$; δ(C16–C111–H)$_{ip}$; δ(C14–C13–H)$_{ip}$; δ(C13–C12–H)$_{ip}$
ν_{24}	–	1055(2)	1123	76	δ(C18–C14–C13)$_{ip}$; δ(C12–C11–C19)$_{ip}$
ν_{25}	1103(m)	–	1116	120	$\rho_{tw}(CH_2)$; δ(C16–C111–H)$_{ip}$
ν_{26}	1028(w)	1028(13)	1048	6	δ(C14–C13–H)$_{ip}$; δ(C12–C11–H)$_{ip}$; δ(C18–C19–H)$_{ip}$
ν_{27}	1006(m)	1004(5)	1008	92	$\rho_{tw}(CH_2)$; ν(C110–Cl); δ(C14–C15–O2)$_{ip}$
ν_{28}	–	–	1007	10	γ(C14–C13–H)$_{iph}$; γ(C13–C12–H)$_{oph}$; γ(C12–C11–H)$_{iph}$
ν_{29}	965(vw)	968(2)	984	1	γ(C14–C13–H)$_{iph}$; γ(C19–C11–H)$_{oph}$; γ(C18–C19–H)$_{iph}$
ν_{30}	943(s)	938(29)	949	35	$\rho_{rock}(CH_2)$; ν(C110–Cl); δ(C12–C11–C19)$_{ip}$; δ(C16–C15–O2)$_{ip}$
ν_{31}	900(vs)	900(4)	899	171	ν(C110–Cl); $\rho_r(CH_2)$; δ(C13–C12–C11)$_{ip}$
ν_{32}	875^{sh}(vw)	–	882	<1	γ(C14–C13–H)$_{iph}$; γ(C13–C12–H)$_{iph}$; γ(C18–C19–H)$_{oph}$
ν_{33}	839(vw)	836(3)	852	17	$\rho_r(CH_2)$; δ(C13–C12–C11)$_{ip}$; ν(C110–Cl)
ν_{34}	803(vw)	800(8)	810	<1	γ(C16–C15–C14); γ(C14–C13–H)$_{iph}$; γ(C13–C12–H)$_{iph}$
ν_{35}	786(m)	786(14)	793	27	δ(C18–O1–C17); ν(C110–Cl)
ν_{36}	766(vs)	768(4)	774	81	γ(C13–C15–H)$_{iph}$; γ(C11–C12–H)$_{iph}$; γ(C19–C11–H)$_{iph}$
ν_{37}	709(m)	708(9)	723	14	γ(C14–C18–C19); γ(C13–C12–C11); γ(C15–C16–C111)
ν_{38}	692(w)	691(11)	700	16	δ(C12–C11–C19); δ(O1–C17–C16); ν(C16–C111)
ν_{39}	670(w)	669(30)	675	13	$\delta(CF_2)$; γ(C18–O1–C17)
ν_{40}	628(vw)	–	640	7	δ(C16–C15–O2); δ(C13–C14–C18); $\delta(CF_2)$
ν_{41}	611(vw)	628(8)	613	16	γ(O1–C17–C16); $\delta_s(CF_2)$; γ(C17–C110–Cl); δ(C11–C19–C18)
ν_{42}	599(vw)	608(51)	594	10	ν(C111–Br)
ν_{43}	577(vw)	579(7)	582	5	δ(C11–C19–C18); δ(C14–C13–C12)
ν_{44}	526(vw)	526(10)	527	3	γ(O1–C18–C19); γ(C13–C12–C11)
ν_{45}	513(vw)	514(33)	518	1	δ(C15–C14–C18); γ(O1–C17–C16)
ν_{46}	475(w)	477(16)	481	28	γ(C16–C111–Br); γ(O1–C17–C16); γ(C18–C19–C11)
ν_{47}	435(vw)	436(17)	439	4	γ(C14–C13–C12); γ(C11–C19–C18)
ν_{48}	426(vw)	–	425	2	γ(F–C110–Cl); δ(O2–C15–C16)$_{ip}$; δ(C19–8a–O1)$_{ip}$
ν_{49}	–	425(13)	418	1	γ(F–C110–Cl); γ(C14–C13–C12); γ(C11–C19–C18)
ν_{50}	–	–	376	9	δ(C16–C15–O2)$_{ip}$
ν_{51}	–	344(15)	345	2	γ(C16–C111–Br); γ(C17–C16–C15)
ν_{52}	–	308(19)	305	3	τ(O1–C18–C14–C15); τ(C15–C16–C111–H)
ν_{53}	–	–	294	1	δ(C14–C18–C19)$_{ip}$
ν_{54}	–	–	292	3	τ(O1–C17–C110–F); γ(C15–C14–C13); $\rho_r(CH_2)$
ν_{55}	–	269(5)	270	2	τ(C13–C12–C11–C19); τ(C13–C14–C18–O1)
ν_{56}	–	192(6)	195	<1	γ(C17–C110–Cl); τ(C16–C17–O1–C18)
ν_{57}	–	168(7)	160	2	δ(O1–C17–C110); τ(C13–C14–C18–O1)
ν_{58}	–	145(14)	130	1	τ(C13–C12–C11–C19); γ(C17–C110–Cl)
ν_{59}	–	–	105	1	γ(C16–C111–Br); τ(C14–C18–O1–C17)
ν_{60}	–	–	61	<1	τ(C18–O1–C17–C16); γ(C17–C110–Cl)
ν_{61}	–	–	46	2	τ(C15–C16–C111–Br); τ(C17–O1–C18–C14)
ν_{62}	–	–	31	<1	τ(C16–CH_2Br)$_{iph}$; τ(C17–CF_2Cl)$_{iph}$
ν_{63}	–	–	28	<1	τ(C17–CF_2Cl)$_{iph}$; τ(C6–CH_2Br)$_{oph}$

[a] vs very strong; s, strong; m, medium; w, weak; vw, very weak; sh, shoulder.
[b] 6-311++g(d,p) calculated IR frequencies (cm^{-1}) and intensities (km mol^{-1}) in parentheses.
[c] ν, δ, γ, τ, ρ_{rock}, ρ_{wag} and ρ_{tw} represent stretching, in-plane deformation, out-of-plane deformation, torsion, rocking, wagging and twisting modes. In phase, in plane and out of phase modes are represented by iph, ip and oph, respectively.

The C–Cl stretching is located at 926 cm^{-1} (IR) and at 918 cm^{-1} in Raman (Calc.: 911 cm^{-1}).

3.4.2. 3-Bromomethyl-2-chlorodifluoromethylchromone (2)

The asymmetric stretching of the CH_2 group was not detected in infrared or Raman and the symmetric stretching was observed as a very weak bands at 2999 cm^{-1} (IR) and 2994 cm^{-1} (Raman). The

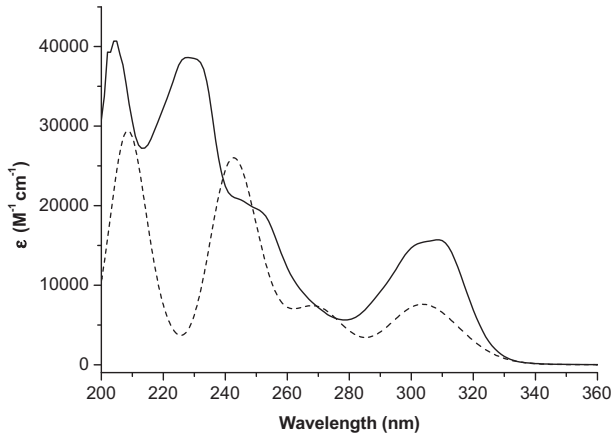

Fig. 9. Experimental (full trace, 4.26×10^{-6} M in methanol) and calculated electronic spectra (B3LYP/6-311++G(d,p), dashed trace) of 2-chlorodifluoromethyl-3-methylchromone (**1**) at room temperature.

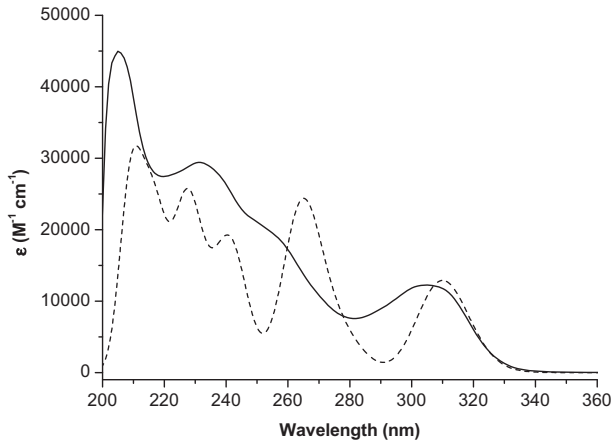

Fig. 10. Experimental (full trace, 3.2×10^{-5} M in methanol) and calculated electronic spectra (B3LYP/6-311++G(d,p), dashed trace) of 3-bromomethyl-2-chlorodifluomethylchromone (**2**) at room temperature.

Table 6
Observed electronic spectrum of 3-methyl-2-chlorodifluoromethylchromone (**1**) in methanol solution along with calculated electronic transitions relevant for the assignments.

Experimental[a]	Calculated[b] (B3LYP/6-311++G (d,p))	Assignment
205	208(0.302)	HOMO−1 → LUMO+2 (95%)
	212(0.128)	HOMO−3 → LUMO+1 (44%) HOMO → LUMO+2 (23%) HOMO−2 → LUMO+2 (14%)
228	242(0.334)	HOMO−3 → LUMO (47%) HOMO → LUMO+1 (45%)
	249(0.070)	HOMO−3 → LUMO (47%) HOMO → LUMO+1 (40%) HOMO−2 → LUMO (10%)
250[c]	269(0.105)	HOMO−2 → LUMO (89%) HOMO → LUMO+1 (11%)
309	304(0.112)	HOMO → LUMO (100%)

[a] Absorption maxima spectral positions are given in nm.
[b] Oscillator strengths of calculated transitions, shown in parenthesis, are in atomic units.
[c] Shoulder.

Table 7
Observed electronic spectrum of 3-bromomethyl-2-chlorodifluoromethylchromone (**2**) along with calculated electronic transitions relevant for the assignments.

Experimental[a]	Calculated[b] (B3LYP/6-311++G (d,p))	Assignment
205	211 (0.253)	HOMO → LUMO+2 (79%) HOMO → LUMO+3 (8%) HOMO−7 → LUMO (7%)
	218 (0.171)	HOMO−5 → LUMO+1 (82%) HOMO−2 → LUMO+2 (10%)
232	227 (0.199)	HOMO−2 → LUMO+1 (64%)
	242 (0.151)	HOMO−5 → LUMO (61%) HOMO−3 → LUMO+1 (20%) HOMO−4 → LUMO+1 (7%)
259[c]	265 (0.204)	HOMO → LUMO+1 (75%)
305	310 (0.123)	HOMO → LUMO (100%)

[a] Absorption maxima spectral positions are given in nm.
[b] Oscillator strengths of calculated transitions, shown in parenthesis, are in atomic units.
[c] Shoulder.

bands at 1432 cm^{-1} (Raman, 1432 cm^{-1}), 1236 cm^{-1} (Raman, 1242 cm^{-1}) and 1175 (Raman, 1173 cm^{-1}) were assigned to the bending, wagging and twisting modes of CH_2 group, respectively. The IR strong band at 943 cm^{-1} (Raman, 938 cm^{-1}) was attributed to the rocking mode of methylene group.

The stretching of the carbonyl (C═O) group appeared as a very strong IR absorption at 1660 cm^{-1} (Calc.: 1713 cm^{-1}) and as a medium intense band in the Raman spectrum at 1672 cm^{-1}. Moreover, the medium IR band at 1631 cm^{-1} (Calc. and Raman at 1656 cm^{-1}) was assigned to the C═C stretching mode of the 4-pyran ring.

The very strong band attributed to the asymmetric stretching mode of the —CF_2 group was observed in the IR spectrum at 1121 cm^{-1} (Calc. 1149 cm^{-1}), while the weak band located at 670 cm^{-1} (Calc.: 675 cm^{-1}) was assigned to the CF_2 group deformation. The C—Cl stretching was attributed to the very strong IR band at 900 cm^{-1} (Calc.: 899 cm^{-1}), and the C—Br stretching to the very weak band located at 599 cm^{-1} (Raman, 608 cm^{-1}).

3.5. Electronic spectra

The experimental and calculated electronic absorption spectra of **1** and **2** were recorded in the 200–1100 nm spectral range, using methanol as solvent (4.26×10^{-6} M for **1** and 3.2×10^{-5} M for **2**) and are shown in Figs. 9 and 10, respectively. In Tables 6 and 7 are presented the main absorption bands, correlated with the calculated values and a tentative assignment of the electronic transitions for **1** and **2**, respectively. Only the dominant transitions ($f > 0.07$ for **1** and $f > 0.12$ for **2**) were taken into account to assign the observed bands.

3.5.1. Molecular orbitals of 1

In Fig. 11, the main molecular orbitals involved in the electronic transitions are depicted. The absorption band observed at 205 nm is due to the contribution of one electron transitions HOMO−1 → LUMO+2 and HOMO−3 → LUMO+1 (Calc. 212 nm). It is originated by excitations from non-bonding orbitals of the oxygen atom of the carbonyl group to the π-antibonding orbitals of the aromatic ring, and from π-bonding orbitals of the aromatic ring and the double bond (C═C) of 4-pyran ring to π-antibonding orbitals of the whole molecule.

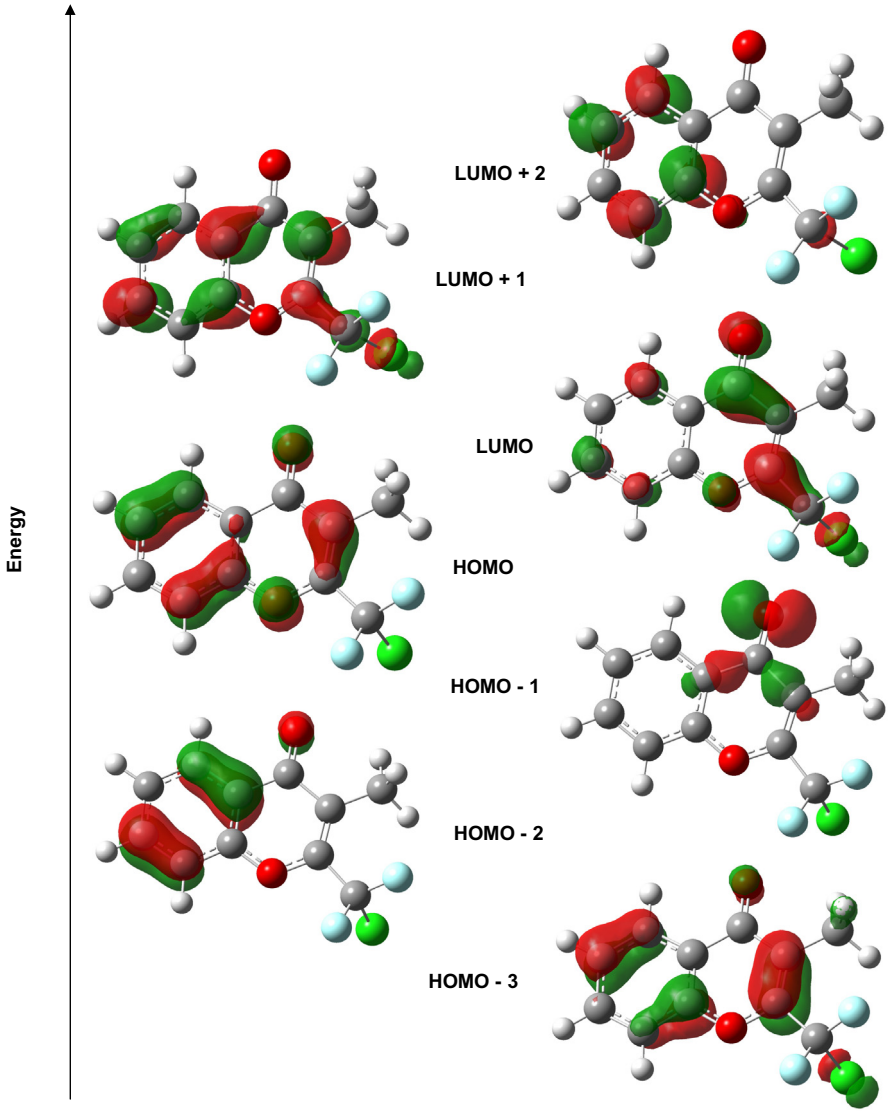

Fig. 11. Molecular orbitals involved in the electronic transitions of 2-chlorodifluoromethyl-3-methylchromone (**1**). The energy scale is only qualitative and does not represent the actual energy of the molecular orbitals.

The absorption at 228 nm is attributed principally to transitions from HOMO−3 → LUMO and HOMO → LUMO+2 orbitals (Calc. 242 and 249 nm). The absorption is generated by excitations from π-bonding orbitals of the aromatic ring and double bond (C=C) of the heterocycle to the π-antibonding orbitals of the aromatic ring and to the non-bonding orbitals of oxygen and chlorine atoms.

The band-shaped shoulder at 250 nm (Calc.: 269 nm) is due to one-electron excitation from HOMO−2 → LUMO orbitals, corresponding to contributions from π orbitals of the aromatic ring and non-bonding orbitals of the oxygen atom (C=O) to the π-antibonding orbitals of the aromatic moiety, double bond (C8=C9) and to the non-bonding orbital of both oxygen and chlorine atoms.

The band at 309 nm (Calc.: 304 nm) is mainly originated by excitations from HOMO to LUMO orbitals, for which the computed energy gap is 4.65 eV. This absorption comes from contributions of π-bonding orbitals of the aromatic ring and double bond (C8=C9) to the π-antibonding orbitals of the aromatic ring and the non-bonding orbitals of both oxygen and chlorine atoms (see Table 5).

3.5.2. Molecular orbitals of 2

Fig. 12 shows the molecular orbitals involved in the electronic transitions. The most intense band, observed in the electronic spectra at 205 nm, is attributed to one-electron transitions from HOMO → LUMO+2 with minor contribution of HOMO−5 → LUMO+1 (Calc. 211 and 218 nm, respectively). This is originated by excitations from the π-bonding orbital of the aromatic ring and C=C double bond, non-bonding orbitals of both oxygen and bromine atoms to the π-antibonding orbital of the aromatic ring, mostly.

The absorption observed at 232 nm (Calc., 227 and 242 nm) is attributed to one-electron transitions from HOMO−2 → LUMO+1 and HOMO−5 → LUMO, on which the relevant electron transitions correspond to excitations $\pi \rightarrow \pi^*$ within the aromatic ring.

The shoulder at 259 nm is dominated by contributions from HOMO → LUMO+1 (Calc.: 265 nm). It is originated by $\pi \rightarrow \pi^*$ transitions within the aromatic moiety and to the non-bonding orbitals of the bromine and oxygen (C=O) atoms.

The absorption at 305 nm (Calc.: 310 nm) is dominated by excitations from HOMO to LUMO orbitals (100%), and involves transitions between π-bonding orbital of the aromatic ring and non-bonding orbital of both oxygen atoms to the π-antibonding orbitals of the whole molecule and non-bonding orbitals of the chlorine atom.

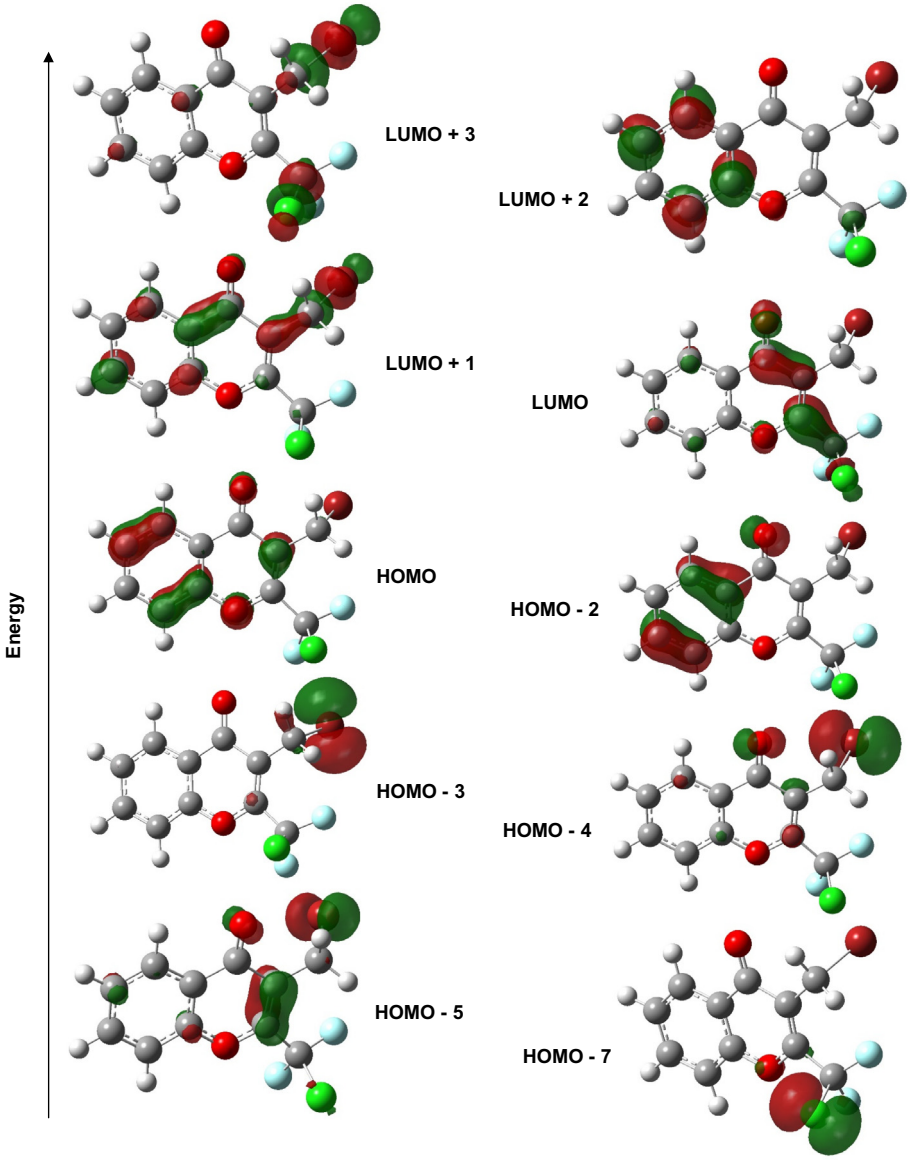

Fig. 12. Molecular orbitals involved in the electronic transitions of 3-bromomethyl-2-chlorodifluomethylchromone (**2**). The energy scale is only qualitative and does not represent the actual energy of the molecular orbitals.

3.6. Fluorescence spectra

Both 2-chlorodifluoromethylchromones were checked for fluorescence. Only the brominated one (**2**) gave measurable signals shown in Fig. 13, all of them excited at 306 nm which is the maximum for the excitation spectrum. The broad band of fluorescence spans from 360 to 550 nm with the maximum at 402 nm. Comparing with the UV absorption spectrum, it is observed that the emission shows itself significantly red-shifted in a region where there is no absorption and therefore there is no overlapping between both signals. This could be an indication that the geometry of the excited state differs appreciably from the one of the ground state, making evident the antibonding character of the promoted electron, as already discussed for the calculation of the UV spectrum.

Fig. 13 also shows that the fluorescence increases with the moles of chromone added to the initial solution, which is 3.86 μM.

In Fig. 13 it can also be seen that the fluorescence increases with the number of moles of chromone added to the initial solution (3.86 μM) up to a point (5 × 3.86 nmoles added) where it reverts and clearly begins to go down with further increments. This

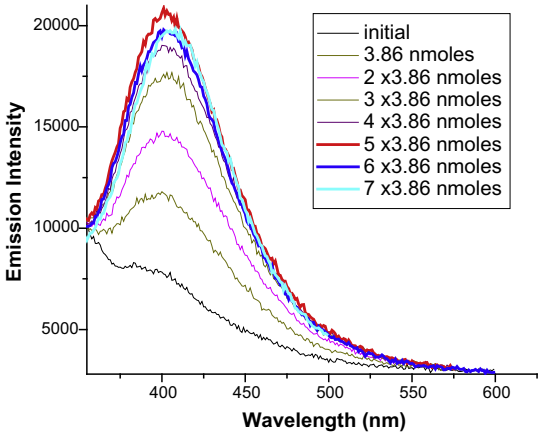

Fig. 13. Fluorescence spectra of **2**, starting at a concentration of 3.86 μM (black trace) and with added solute in amounts of 3.86 nmoles each. The red trace indicates the maximum and the following two (blue and cyan) wider traces show diminution of intensity. (For interpretation of the references to colour in this figure legend, the reader is referred to the web version of this article.)

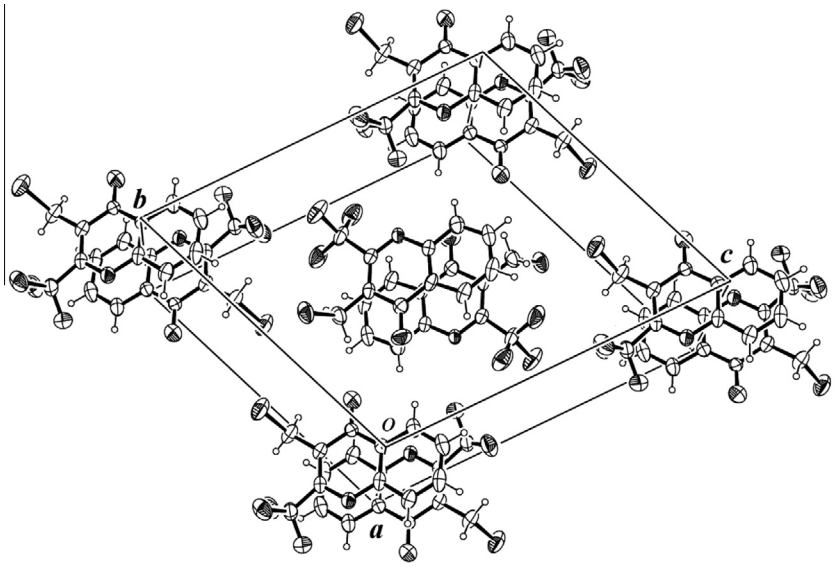

Fig. 14. Crystal packing of **2**, showing neighboring inversion relatedmolecules stacking along the *a*-axis.

Table 8
Comparison between experimental and B3LYP calculated NMR chemical shifts (in ppm) for **1** and **2**.[a]

	1				**2**		
	Exp.	6-311+g(2d,p)			Exp.	6-311+g(2d,p)	
C<u>H</u>$_3$	2.24	2.25	(−0.01)	C<u>H</u>$_2$	4.61	4.96	(−0.35)
5-H	8.18	8.65	(−0.47)	5-H	8.24	8.64	(−0.40)
6-H	7.42	7.65	(−0.23)	6-H	7.50	7.66	(−0.16)
7-H	7.71	7.88	(−0.17)	7-H	7.79	7.90	(−0.11)
8-H	7.49	7.66	(−0.17)	8-H	7.55	7.69	(−0.14)
2-C	151.8	160.1	(−8.3)	2-C	153.5	161.2	(−7.7)
3-C	118.9	127.7	(−8.8)	3-C	119.3	127.5	(−8.2)
4-C	178.1	181.4	(−3.3)	4-C	175.7	179.3	(−3.6)
5-C	125.9	132.7	(−6.8)	5-C	126.7	132.9	(−6.2)
6-C	126.2	129.7	(−3.5)	6-C	126.5	130.6	(−4.1)
7-C	134.6	138.2	(−3.6)	7-C	135.3	139.25	(−3.9)
8-C	118.2	121.9	(−3.7)	8-C	118.4	122.2	(−3.8)
4a-C	122.2	128.4	(−6.2)	4a-C	122.5	128.5	(−6.0)
8a-C	154.9	161.6	(−6.7)	8a-C	154.8	161.4	(−6.6)
C<u>H</u>$_3$	9.0	10.7	(−1.7)	C<u>H</u>$_2$Br	19.3	36.1	(−16.8)
C<u>F</u>$_2$Cl	121.8	139.0	(−17.2)	C<u>F</u>$_2$Cl	121.2	139.23	(−18.0)

[a] $\delta = \delta_{exp} - \delta_{calc}$ values in parentheses. The standard numbering scheme of the benzopyran skeleton was adopted for atoms labeling.

decrease evidences a diminution in the number of emitters that could be explained either as a quenching, autoabsorption or an association. Since no other molecules were added to the solution but the solute itself; the autoabsorption could in principle be discarded (negligible absorption cross section at the wavelength of fluorescence), then we conclude that the most likely process would be intramolecular interaction to form dimers. This is supported by the observed crystal packing, where neighboring inversion related molecules stacks along the *a*-axis with alternated short contacts of about 3.5 and 3.8 Å such as to favor π–π intermolecular interaction between the fused rings (see, Fig. 14).

3.7. Theoretical and experimental NMR spectroscopy

The calculated ^{1}H and ^{13}C chemical shifts (δ) were performed with the GIAO method,[56] after full geometry optimization with the GAUSSIAN 03 program.[48] Table 8 shows the comparison between experimental and calculated values. The linear relationship between calculated and experimental data gives R-square values above 0.997 for **1**, and 0.992 for **2**. The correlation [$\delta_{calc} = a\,\delta_{exp} + b$] given in Fig. S5(a–d) (Supporting Information) were obtained with the following results: Fig. **a**, ^{1}H NMR: ($R^2 = 0.997$; $a = 1.050$; $b = -0.129$); Fig. **b**, ^{13}C NMR: ($R^2 = 0.998$; $a = 1.022$; $b = 2.493$) for **1**; Fig. **c**, ^{1}H NMR: ($R^2 = 0.998$; $a = 0.969$; $b = 0.452$), and Fig. **d**, ^{13}C NMR: ($R^2 = 0.992$; $a = 0.990$; $b = 6.906$) for **2**. Comparing the experimental and theoretical data for protons, a good agreement is observed with $\Delta = \delta_{exp} - \delta_{calc}$ deviation ranging from −0.47 to 0.01 and from −0.40 to −0.11 ppm for **1** and **2**, respectively.

However, the deviation Δ-values found for the carbon atoms rise up to 18.0 ppm (see Table 7). The greatest discrepancies were found in the prediction of the –C<u>F</u>$_2$Cl ($\Delta = 17.2$ and 18.0 ppm, for **1** and **2**, respectively), and –C<u>H</u>$_2$Br chemical shifts ($\Delta = 16.8$ ppm for **2**). The observed differences could be attributed to the well documented heavy atom effect, even for chlorine atom, since the GIAO method neglect relativistic effects as stated by Dybiec and Gryff-Keller [57]. Similar deviations were outlined in a previous work [14], and also reported in related halogenated compounds [58].

Furthermore, calculations also failed to describe correctly the experimental data of α-carbon atoms for the chlorodifluoromethyl group with $\Delta = 8.3$ and −7.7 ppm for **1** and **2**, respectively (see Table 7). Here, the observed discrepancies could be due to the additional effect of the chlorine, as heavy atom, and to the isotropic shielding of the two fluorine atoms [59,60]. However, the experimental chemical shift values (^{13}C NMR) for –C<u>F</u>$_2$Cl (**1** and **2**) and –C<u>H</u>$_2$Br (**2**) are in good agreement with molecules containing the same structural portions.

4. Conclusions

The calculated vibrational (IR and Raman) and electronic spectra of **1** and **2** are in good accordance with the experimental data, supporting the assignment of the observed bands. The GIAO approach was suitable for predicting the ^{1}H and ^{13}C chemical shifts in both compounds, but underestimates the isotropic shielding of the heavy chlorine and bromine atoms, whose relativistic effects are not considered in the in the GIAO calculations and also the strong electron-withdrawing effect of the fluorine atoms. As noted by quantum chemical calculations and X-ray crystal structure

results, both title compounds exhibit planar conformations due to a large π-bonding conjugation, which extends almost along the whole molecule. Particularly for **2**, the presence of "halogen bonding" interactions prevail in the geometry adopted in the solid phase, which differs from that predicted by theoretical calculations. The calculated and experimental structural parameters are also in good agreement, showing that no drastic changes occurs going from solid to gas phase. Fluorescence spectroscopy was valuable to understand the differences between the more stable conformer (predicted by theoretical calculations) and that found in the crystal for compound **2**. This molecule gave measurable signals when irradiated with $\lambda_{exc.}$ = 306 nm. The proposed association due to intermolecular interactions, when chromone concentration was increased, is in accordance with the short contacts found in the crystal packing, to promote π–π intermolecular interaction between the fused rings. These positive associative effects and the small ΔE difference between conformers are apparently decisive to favor the conformation of higher energy (with the halogen atoms at the same side) to form the crystal.

Conflict of interest

The authors declare no conflict of interest in this paper.

Acknowledgements

The authors thank Universidad Nacional de La Plata (UNLP), CONICET, DAAD-Germany, and Departamento de Ciencias Básicas de la Universidad Nacional de Luján for financial support. S.E.U and J.L.J specially thanks Deutscher Akademischer Austauschdienst Germany (DAAD) for an equipment grant and financial support. CDAL thanks SENESCYT for the fellowship and financial support. This work was supported by CONICET (PIP 1529 and 0359), and by ANPCyT (PME06 2804 and PICT06 2315) of Argentina. S.E.U., G.A.E., O.E.P, M.P.B. and G.A.A. are Research Fellows of CONICET.

Appendix A. Supplementary data

Supplementary data associated with this article can be found, in the online version, at http://dx.doi.org/10.1016/j.chemphys.2016.03.017.

References

[1] G.P. Ellis, Naturally Occurring Chromones, Chemistry of Heterocyclic Compounds, John Wiley & Sons Inc., Hoboken, NJ, USA, 2008. pp. 455–480.
[2] A.G. Andrei, L.K. Kenneth, Fluorinated Heterocycles, Fluorinated Heterocycles, American Chemical Society, 2009, pp. 3–20.
[3] G. Sandford, Perfluorinated Six-Membered Aromatic Heterocycles Containing One or More Heteroatom, Fluorinated Heterocyclic Compounds, John Wiley & Sons Inc., 2009. pp. 303–324.
[4] M.T. Giardi, G. Rea, B. Berra, Bio-Farms for Nutraceuticals: Functional Food and Safety Control by Biosensors, Landes Bioscience, 2010.
[5] G.G. Chabot, Y.S. Touil, M.H. Pham, D. Dauzonne, Flavonoids in cancer prevention and therapy: chemistry, pharmacology, mechanisms of action, and perspectives for cancer drug discovery, in: M. Alaoui-Jamali (Ed.), Alternative and Complementary Therapies for Cancer, Springer, USA, 2010, pp. 583–612.
[6] E.S.C. Wu, J.T. Loch, B.H. Toder, A.R. Borrelli, D. Gawlak, L.A. Radov, N.P. Gensmantel, J. Med. Chem. 35 (1992) 3519.
[7] X. Wu, S. Yin, J. Zhong, W. Ding, J. Wan, Z. Xie, Fitoterapia 83 (2012) 1706.
[8] B. China, R. Raju, Bioorg. Med. Chem. Lett. 21 (2011) 2855.
[9] J. Ungwitayatorn, C. Wiwat, W. Samee, P. Nunthanavanit, N. Phosrithong, J. Mol. Struct. 1001 (2011) 152.
[10] Y. Chen, H.-R. Liu, H.-S. Liu, M. Cheng, P. Xia, K. Qian, P.-C. Wu, C.-Y. Lai, Y. Xia, Z.-Y. Yang, S.L. Morris-Natschke, K.-H. Lee, Eur. J. Med. Chem. 49 (2012) 74.
[11] A.Y. Shaw, C.-Y. Chang, H.-H. Liau, P.-J. Lu, H.-L. Chen, C.-N. Yang, H.-Y. Li, Eur. J. Med. Chem. 44 (2009) 2552.
[12] J.T. Welch, Tetrahedron 43 (1987) 3123.
[13] G.A. Patani, E.J. LaVoie, Chem. Rev. 96 (1996) 3147.
[14] C.D. Alcívar León, G.A. Echeverría, O.E. Piro, S.E. Ulic, J.L. Jios, Spectrochim. Acta A 136 (2015) 1358–1370.
[15] G.R. Desiraju, R. Parthasarathy, J. Am. Chem. Soc. 111 (1989) 8725.
[16] V.R. Pedireddi, D.S. Reddy, B.S. Goud, D.C. Craig, A.D. Rae, G.R. Desiraju, J. Chem. Soc., Perkin Trans. 2 (1994) 2353.
[17] F.H. Allen, O. Kennard, Chem. Des. Autom. News 8 (1993) 31.
[18] P. Metrangolo, G. Resnati, T. Pilati, R. Liantonio, F. Meyer, J. Polym. Sci. A Polym. Chem. 45 (2007) 1.
[19] P. Metrangolo, F. Meyer, T. Pilati, G. Resnati, G. Terraneo, Angew. Chem., Int. Ed. 47 (2008) 6114.
[20] A.C. Legon, Angew. Chem., Int. Ed. 38 (1999) 2686.
[21] G.R. Desiraju, Nature 412 (2001) 397.
[22] P. Metrangolo, G. Resnati, Chem. Eur. J. 7 (2001) 2511.
[23] E. Bosch, C.L. Barnes, Cryst. Growth Des. 2 (2002) 299.
[24] C.B. Aakeröy, P.D. Chopade, J. Desper, Cryst. Growth Des. 11 (2011) 5333.
[25] D. Braga, L. Brammer, N.R. Champness, CrystEngComm 7 (2005) 1.
[26] J.A.R.P. Sarma, F.H. Allen, V.J. Hoy, J.A.K. Howard, R. Thaimattam, K. Biradha, G. R. Desiraju, Chem. Commun. 101–102 (1997).
[27] J. Hulliger, P.J. Langley, Chem. Commun. (1998) 2557.
[28] P.K. Thallapally, G.R. Desiraju, M. Bagieu-Beucher, R. Masse, C. Bourgogne, J.-F. Nicoud, Chem. Commun. (2002) 1052.
[29] E. Cariati, A. Forni, S. Biella, P. Metrangolo, F. Meyer, G. Resnati, S. Righetto, E. Tordin, R. Ugo, Chem. Commun. (2007) 2590.
[30] T.-R. Tero, K. Salorinne, M. Nissinen, CrystEngComm 14 (2012) 7360.
[31] K.L. Kirk, Org. Process Res. Dev. 12 (2008) 305.
[32] B.E. Smart, J. Fluorine Chem. 109 (2001) 3.
[33] M.I. Lvovskaya, A.D. Roshal, A.O. Doroshenko, A.V. Kyrychenko, V.P. Khilya, Spectrochim. Acta A 65 (2006) 397.
[34] J.R. Zimmerman, O. Johntony, D. Steigerwald, C. Criss, B.J. Myers, D.H. Kinder, Org. Lett. 17 (2015) 3256.
[35] A.S. Klymchenko, V.G. Pivovarenko, T. Ozturk, A.P. Demchenko, New J. Chem. 27 (2003) 1336.
[36] S. Hofener, P.C. Kooijman, J. Groen, F. Ariese, L. Visscher, Phys. Chem. Chem. Phys. 15 (2013) 12572.
[37] S.M. Beyhan, A.W. Götz, F. Ariese, L. Visscher, C. Gooijer, J. Phys. Chem. A 115 (2011) 1493.
[38] I.Y. Martynov, V.A. Barachevsky, A.O. Ayt, O.I. Kobeleva, T.M. Valova, K.S. Levchenko, V.N. Yarovenko, M.M. Krayushkin, Opt. Mater. 37 (2014) 488.
[39] I.S. Semenova, K.S. Levchenko, V.N. Yarovenko, M.M. Krayushkin, V.A. Barachevskii, O.I. Kobeleva, T.M. Valova, Russ. Chem. Bull. 61 (2012) 1761.
[40] J. Miao, H. Cui, J. Jin, F. Lai, H. Wen, X. Zhang, G.F. Ruda, X. Chen, D. Yin, Chem. Commun. 51 (2015) 881.
[41] S.E. Kharrat, R.E. Kharrat, P. Laurent, H. Blancou, Synthesis 2007 (2007) 3542.
[42] K. Tamura, T. Ishihara, H. Yamanaka, J. Fluorine Chem. 68 (1994) 25.
[43] L.P. Avendaño Jiménez, G.A. Echeverría, O.E. Piro, S.E. Ulic, J.L. Jios, J. Phys. Chem. A 117 (2013) 2169.
[44] I.C. Henao Castañeda, S.E. Ulic, C.O.D. Védova, N. Metzler-Nolte, J.L. Jios, Tetrahedron Lett. 52 (2011) 1436.
[45] CrysAlisPro, Oxford Diffraction Ltd., 2009.
[46] G. Sheldrick, Acta Crystallogr. Sect. A 64 (2008) 112.
[47] H. Flack, Acta Crystallogr. A 39 (1983) 876.
[48] M.J. Frisch, G.W. Trucks, H.B. Schlegel, G.E. Scuseria, M.A. Robb, J.R. Cheeseman, J.A. Montgomery Jr., T. Vreven, K.N. Kudin, J.C. Burant, J.M. Millam, S.S. Iyengar, J. Tomasi, V. Barone, B. Mennucci, M. Cossi, G. Scalmani, N. Rega, G.A. Petersson, H. Nakatsuji, M. Hada, M. Ehara, K. Toyota, R. Fukuda, J. Hasegawa, M. Ishida, T. Nakajima, Y. Honda, O. Kitao, H. Nakai, M. Klene, X. Li, J.E. Knox, H. P. Hratchian, J.B. Cross, C. Adamo, J. Jaramillo, R. Gomperts, R.E. Stratmann, O. Yazyev, A.J. Austin, R. Cammi, C. Pomelli, J.W. Ochterski, P.Y. Ayala, K. Morokuma, G.A. Voth, P. Salvador, J.J. Dannenberg, V.G. Zakrzewski, S. Dapprich, A.D. Daniels, M.C. Strain, O. Farkas, D.K. Malick, A.D. Rabuck, K. Raghavachari, J.B. Foresman, J.V. Ortiz, Q. Cui, A.G. Baboul, S. Clifford, J. Cioslowski, B.B. Stefanov, G. Liu, A. Liashenko, P. Piskorz, I. Komaromi, R.L. Martin, D.J. Fox, T. Keith, M.A. Al-Laham, C.Y. Peng, A. Nanayakkara, M. Challacombe, P.M.W. Gill, B. Johnson, W. Chen, M.W. Wong, C. Gonzalez, J.A. Pople, Gaussian 03, Gaussian Inc., Pittsburgh PA, 2003.
[49] A. Dreuw, M. Head-Gordon, Chem. Rev. 105 (2005) 4009.
[50] P. Elliott, F. Furche, K. Burke, Excited States from Time-Dependent Density Functional Theory, Reviews in Computational Chemistry, John Wiley & Sons Inc., 2009, pp. 91–165.
[51] V. Barone, M. Cossi, J. Phys. Chem. A 102 (1998) 1995.
[52] M. Cossi, N. Rega, G. Scalmani, V. Barone, J. Comput. Chem. 24 (2003) 669.
[53] L. Farrugia, J. Appl. Cryst. 30 (1997) 565.
[54] W. Kabsch, Acta Crystallogr. Sect. A 32 (1976) 922.
[55] G. Desiraju, T. Steiner, The Weak Hydrogen Bond in Structural Chemistry and Biology, IUCr Monographs on Crystallography, vol. 9, Oxford University Press, Oxford, 1999.
[56] R. Ditchfield, Mol. Phys. 27 (1974) 789.
[57] K. Dybiec, A. Gryff-Keller, Magn. Res. Chem. 47 (2009) 63.
[58] A.C. Neto, L.C. Ducati, R. Rittner, C.F. Tormena, R.H. Contreras, G. Frenking, J. Chem. Theory Comput. 5 (2009) 2222.
[59] I. Cakmak, J. Mol. Struct. (THEOCHEM) 716 (2005) 143.
[60] K.G. Andrews, A.C. Spivey, J. Org. Chem. 78 (2013) 11302.